AD-A191 851 OBSERVATIONS OF FRONTAL INSTABILITIES ON AN UPWELLING FFILAMENT(U) UNIVERSITY OF SOUTHERN CALIFORNIA LOS ANGELES CENTER FOR EARTH SCIENCES L WASHBURN ET AL. 1/1

UNCLASSIFIED 1987 N00014-87-K-0220 F/G 8/3 NL

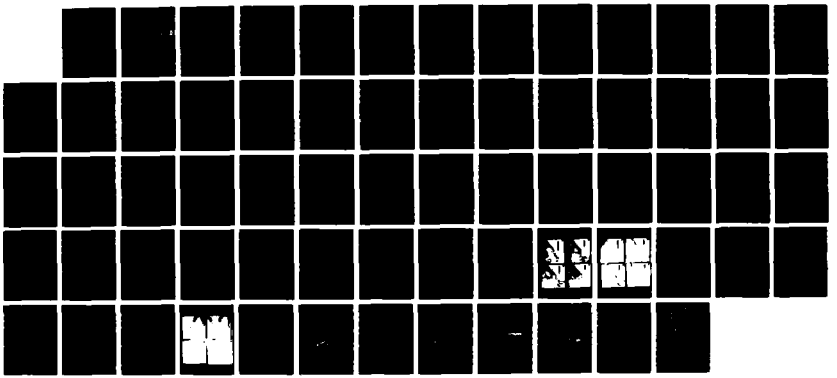

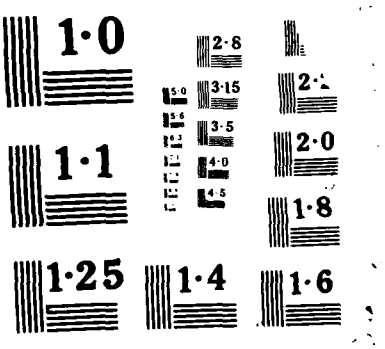
1·0
1·1
1·25
1·4
1·6
1·8
2·0
2·2
2·5
3·15
3·5
4·0
4·5

(4)

Contract N00014-87-K-0220

Observations of frontal instabilities on an upwelling filament

Libe Washburn

Ocean Physics Group

Center for Earth Sciences

University of Southern California

Los Angeles, CA 90089-0741

Laurence Armi

Scripps Institution of Oceanography

La Jolla, CA 92093

(Submitted to the Journal of Physical Oceanography)

Abstract

Frontal instabilities were observed along a density front on the cyclonic boundary of an upwelling filament which formed north of Pt. Arguello, California in October 1983. Observations of the instabilities were conducted using satellite sea surface temperature images and in situ sampling. The instabilities formed on the southern (cyclonic) boundary of the filament at a wavelength of about 20 km and consisted of two lobes, one warm and one cool, each with a width of about 4 km. The time scale for formation of the instabilities is about 1 day. Near surface distributions of temperature, salinity, and density within the cool lobes of the instabilities are consistent with local upelling at the rate of about 30 m/d. A simple model based on conservation of potential vorticity is presented which accounts for the observed upwelling. Based on isopycnal displacements and the distribution of salinity, the signature of the instabilities appears to be confined to the upper 50 m of the water column.

1. Introduction

Upwelling filaments are commonly observed features along the west coast of the North America and are important mechanisms for transporting coastally upwelled water far offshore beyond the continental shelf. The vertical structure of these filaments is that of a surface intensified, baroclinic jet (Flament, et al 1985; Reinecker, et al 1985) with maximum offshore surface velocities exceeding 0.5 m/s (Kosro, 1987; Huyer and Kosro, 1986). Velocity surveys employing surface drifters (Davis, 1985) and Doppler acoustic current profilers (Kosro, 1987) with contemporaneous satellite sea surface temperature (SST) images indicate that these high offshore surface velocities often occur in association with cool filaments which extend offshore up to 200 km. The time scale of these filaments, based mainly upon SST imagery, appears to be on the order of a few weeks to several weeks, although the details of their growth and decay are largely unknown at present. Recent laboratory experiments in a rotating tank have shown that plume-like features resembling upwelling filaments can form in association with bottom topography such as a ridge (Narimousa and Maxworthy, 1985). Other experiments (Narimousa and Maxworthy, 1987) have shown that plume-like features can also result from baroclinic instability of an upwelling front in the absence of bottom topography. These features in the latter experiments were non-stationary and occurred randomly along the upwelling front.

To date, the occurrence of these filaments has been most completely documented along the California coast north of San Francisco, particularly in the CODE region. However, they are not limited to this portion of the coast. Temperature structures which resemble upwelling filaments often form off central California. For example, an irregular region of relatively cool surface water (about 2 ^{o}C cooler than surrounding water) extending about 80 km southward from Pt. Conception is present in the 12 October 1984 image reported by Chelton et al (1987). Another SST image obtained by Sheres and Kenyon (1987) from 14 May 1984 shows a cool region resembling a filament that extends at least 100 km offshore just north of Pt. Arguello.

This paper presents observations of an upwelling filament which formed off the central California coast during October 1983. From the SST imagery, the filament appears to be rooted north of Pt. Argeullo in roughly the same coastal region as the filament in the image of Sheres and Kenyon (1987). A sequence of SST images was obtained which shows the growth and decay of the surface temperature field of the filament over a two week period. In situ measurements show that the offshore extent and volume transport of this filament are similar to those of filaments off the northern California coast.

A primary objective of the in situ sampling of this experiment was to observe the formation and evolution of transient, coherent structures which often form in association

with upwelling filaments, but which are also observed in oceanic flows generally. Of particluar interest are instabilites which are observed on frontal boundaries and which may be important in the dissipation of kinetic energy and in the horizontal exchange of heat, mass, and momentum in the upper ocean. During the experiment described in this paper, near surface tow-yo transects through the upper 100 m of the water column were conducted across a pair of frontal instabilities which were observed on the cyclonic boundary of the filament. The term instability is used here to characterize these features because their amplitudes grow in time and because their evolution and development are at least superficially similar to shear instabilities observed in laboratory flows. Comparable images of shear instabilities were reported by Flament and Armi (1985). Frontal eddies or "shingles" have been observed on larger scales (100 to 200 km) along the cyclonic front of the Gulf Stream (Lee et al, 1981; Lee, 1975; Lee and Mayer; 1977; Lee and Atkinson; 1983). Cyclonic eddies observed by Kennelly et al (1986) on the boundary of a warm-core ring also appear to be similar to the instabilities observed on this filament, although the eddies which they observed were larger both horizontally and vertically and had longer lifetimes.

A major difficulty in sampling these transient features is that their appearance cannot be assured for a particular experiment nor can their location be predicted. Therefore, considerable flexibility must be incorporated into the

experimental design if they are to be observed by methods other than satellite SST imagery. Real time direction of shipboard sampling is also an essential element of the observing plan. The details of the experiment and instrumentation are given in Section 2. A line of CTD stations across the filament is used to examine the water mass characteristics and to compute a section of the geostrophic velocity field across the filament. These observations of the large scale structure of the filament are discussed in Section 3. Sections 4 and 5 deal with the SST imagery of the instability evolution and with the tow-yo transects across the instabilities. Simple conceptual models to explain some of the details of the near surface finestructure and property distributions are also given.

2. Experimental description and data processing

In situ CTD data of this paper were collected northeast of Pt. Arguello, California on 22 and 23 October 1983. In addition, satellite SST images of this region were obtained over a two week period from 11 to 25 October 1983 and are used to examine the evolution and decay of the filament. During the sea going portion of this experiment these images were received at the Scripps satellite facility and transmitted to the R/V Ellen B. Scripps via radiotelephone and telecopiers and used to direct the in situ sampling.

The instrument platform carries a Neil Brown Instrument Systems CTD and consists of a section of steel channel which has a large fin protruding rearward to maintain the orientation of the CTD sensors into the flow as the platform is moved through the water. This platform has been used on several cruises and is stable at the low tow speeds of this experiment; a drawing of the platform is given by Washburn and Deaton (1986). Sections of temperature (T), salinity (S), and potential density anomaly (σ_θ) are obtained from "tow-yo's" by winching the instrument package vertically at about .6 m/s with the ship underway at about 1.5 m/s. Continuous sea surface water properties are obtained by pumping seawater from a depth of about 2 m through a small chamber on deck which contains a Neil Brown conductivity cell and a platinum resistance thermometer. However, during this experiment, excessive bubble formation in the chamber resulted in unusable surface salinity and density data; the surface temperature data is unaffected by this problem. The transit time of the water through the pumping system is sufficiently rapid such that no measurable heating or cooling of the water occurred. During the in situ sampling the wind speed was typically about 10 m/s from 310^{o} (along coast and upwelling favorable) as shown in the upper plot of Figure 1. The surface mixed layer was consistently about 30 m deep, so both the 2 m pumped temperature data and the satellite SST images give representative temperatures for the surface layer. Wind data of Figure 1 are from the ship's log in which wind speed and direction are

recorded every 2 hr.

Conductivity, temperature, and pressure are recorded at 32 Hz and logged on nine track tape at sea. Absolute calibration of salinity is based upon in situ bottle sampling while temperature calibration is based upon measurements from reversing thermometers and pre-cruise and post-cruise laboratory calibration. The results of this paper are mainly dependent on relative changes in temperature and salinity; significant relative changes for temperature and salinity are conservatively estimated to be 0.01 $^{\circ}$C and 0.001, respectively. During post-cruise processing conductivity data are filtered with a 1-pole low pass digital filter with an effective analog time constant of 0.1 s. This time constant was found to minimize salinity spiking in most sections of the data records, although some residual spikes remain. Because of the constantly varying platform speed, a single value of this time constant will not be ideal for all of the data. After filtering the conductivity data, one second running means of temperature, conductivity, and pressure are formed and subsampled to a point about every 0.5 s. These running means are used to compute salinity and density. Further smoothing is obtained by averaging all variables into "pressure bins" of 2 dbar. Erroneously large and small values of salinity and density due to residual spiking are detected during processing and are not included in the 2 dbar averages. Vertical gradients of temperature, salinity, and density are obtained from a centered, first difference between adjacent 2 dbar averages of

these quantities.

Ship's position from a LORAN receiver is logged continuously throughout the experiment every 20 s and is used to convert time to distance for the production of two dimensional maps of property sections. Relative distance along a particular ship track as a function of time is obtained from smoothed values of latitude and longitude and is interpolated from a piece-wise linear fit to the position data. Occasional "dropouts" are found in the LORAN data and during these times position is reconstructed by linear interpolation. Dropouts occur in less that 5% of the position data.

3. Large scale development and structure of filament

A sequence of four satellite infrared images of the distribution of SST covering the area northwest of Pt. Arguello over a two week period is shown in Figures 2A, B, C, and D. Dark areas indicate relatively warm waters and light areas are cooler waters. Maximum SST differences in the images are about 4 ^{o} C. Spacing between tic marks in the images is one degree in both latitude and longitude. The first image in the sequence, Figure 2A, is from 23:30 GMT on 11 October (JD 284) and shows cold water associated with the upwelling center located between Pt. Conception (identified as PC in Figure ?C) and Pt. Arguello (PA).

The upwelling center evident in this image is a recurring feature of this region of the California coast and is similar in extent to that observed by Atkinson et al (1986) during the OPUS experiment. A broad region of relatively warmer surface water may be seen offshore from the upwelling center; this warm water extends northward past Pt. Buchon (PBu) and is suggestive of a northward coastal flow. Other observations discussed by Chelton et al (1987) indicate that the warm, northward flowing "Davidson Current" is seasonally present along this section of the coast beginning in September or October. The broad light colored area along the western boundary of the image is a layer of clouds.

A very different pattern of SST is seen in the second image of the sequence, Figure 2B, taken at 22:17 on 17 October (JD 290). The upwelling center at Pt. Conception is absent in this image with warmer surface waters replacing the cooler upwelled waters at the coastline. The offshore region of warmer water visible in Figure 2A is still present, but is bisected by the developing filament of colder water which extends offshore along 34^{o} $50^{'}$. In the third image taken at 11:37 on 22 October (JD 295) the SST expression of the filament extends about 120 km offshore with a width of about 50 km. The boundaries of the filament are most clearly defined in this image compared with any of the other cloud-free images obtained over the two week period of these observations. The CTD tow-yo surveys of the filament discussed in Section 4 were conducted over a 25 h period which includes the time when this image was taken. Clouds are found in

the image along the coast immediately north of Pt. Conception and around the Channel Islands in the lower right hand corner.

In the final image of the sequence taken at 15:14 on 25 October the well defined filament structure of the previous image has been replaced with irregular elongated patches of cool water. A broad region of cool surface water which is present at the coast north of Pt. Buchon in Figure 2C has extended farther south in Figure 2D. Based on the SST expression, the time scale for formation and decay of this filament is about two weeks, although the velocity field associated with the feature may have a different timescale.

In order to examine the sub-surface distribution of temperature, salinity, and density across the filament, a section of CTD stations was obtained along the ship track shown superimposed on the SST image of Figure 2C. A time line which summarizes the sequence of the CTD stations, tow-yo sections, satellite imagery, and wind conditions for the time period 00:00 GMT on 22 October to 16:00 on 23 October, 1983 is given in Figure 1. The time interval during which the section of CTD stations was obtained is labeled S1 in Figure 1 and extends from 03:01 to 18:32 on 22 October 1983 (Julian Day, JD 295). The arrow above the time line labeled I2 marks the time when the SST image of Figure 2C was taken; this occurs about midway through the time interval S1. The entire sequence of images I1-I4 with an average spacing of about 6 hr is discussed in Section 4. The intended

ship track was a straight line between the end points of the actual track which is shown in Figure 2C; however, the ship was apparently deflected to the west by the near surface velocity field of the filament.

The maximum sampling depth of each CTD station is about 500 m with an average spacing of 5.5 km. A contour section of temperature to 500 dbar is given in Figure 3A with a contour interval of 0.5 ^{o}C. Tic marks and numbers along the top of the figure identify the location of the 10 CTD stations. North is to the left and the x-axis gives relative distance along the ship track. Surface temperatures decrease over the first half of the section and reach a minimum of about 15.25 ^{o}C at Station 5. Farther along the section, surface temperatures rise steadily reaching a maximum of 18.2 ^{o}C in the warm water just south of the filament. A consistent tilting of the isotherms is evident below about 50 dbar with isothermal surfaces shoaling to the south. The 8 ^{o}C isotherm, for example, rises by about 60 m over the 50 km width of the section giving an average isotherm slope of about 10^{-3}. Salinity contoured along the same section with an isohaline spacing of 0.05 is shown in Figure 3B. At the surface, salinity increases monotonically from north to south reaching a maximum value of about 33.41 at Station 10. Below 250 dbar vertical salinity gradients are generally low within the filament, although a weak salinity maximum is present in Station 8 at about 300 dbar. Overall the filament waters are free of obvious thermohaline intrusions above 500 dbar and are

diffusively stable in the mean.

Potential density anomaly σ_θ is contoured in Figure 3C for the section with a contour interval of 0.05 kg/m^3. The map is very similar to the temperature map of Figure 3A because the filament waters are thermally stratified. As with temperature, a consistent tilt of the isopycnals across the section is evident below 50 dbar. An upward doming of isopycnal surfaces which is coherent vertically over about 100 dbar may be seen centered at 120 dbar at about 14 km into the section.

Density profiles along the line of CTD stations are used to construct contours of the geostrophic flow field referenced to 480 dbar across this part of the filament. To produce a smoothed estimate of geostrophic velocity relative to 480 dbar at a given station, profiles of geopotential anomaly from stations on either side are differenced. The spacing between stations used in computing geostrophic velocity is typically about 10 km. Examples of these profiles from three stations across the filament are shown in Figure 4A. Positive velocity indicates onshore flow. A profile is identified in Figure 4A by the stations which are used to produce it; profile 1-3, for example, is obtained from geopotential anomaly profiles at Stations 1 and 3. Maximum relative current velocities of -.38 m/s are found for this profile at around 60 dbar and the vertical velocity structure of the filament is that of an offshore jet with velocity increasing in the upper water column. The velocity with

respect to 480 dbar increases to zero at around 300 dbar and is positive everywhere below. The second profile 5-7 in Figure 4A has roughly the same shape as profile 1-3 except that the velocity maximum is only about -.16 m/s and the flow with respect to 480 dbar is offshore throughout the profile. The third profile 8-10 located at the SST front on the southern end of the line of CTD stations indicates an onshore return flow everywhere below 70 dbar with maximum velocities of about .05 m/s. Onshore flow probably extends all the way to the surface south of the SST front as suggested by a velocity profile computed between Stations 9 and 10 which are more representative of conditions south of the filament. A portion of this profile to 250 dbar is shown with a dotted line in Figure 4A and indicates onshore flow everywhere above 480 dbar. In Figures 3A and 3B, it can be seen that the mean slope of isotherms and isopycnals is smaller between these two stations consistent with a weakening offshore geostrophic flow at the filament boundary. It should be pointed out, however, that the distance between Stations 9 and 10 is only about 4.5 km; at small scales internal waves can contribute as much or more to local isopycnal gradients as the larger scale geostrophic flow.

The geostrophic velocity contours of Figure 4B, which are computed from profiles as described above, show a near surface maximum at the northern end of the section and indicate that the velocity field of the filament was not completely crossed in this section. Another more narrow surface velocity maximum is found

near the southern end of the cross section at about 40 km. The maximum relative velocity here is about .30 m/s and is just north of the boundary between the offshore flow of the filament and the weak onshore return flow to the south. Onshore flow in Figure 4 is indicated by stippling and maximum onshore current velocities which exceed .05 m/s are found at 200 dbar in the region of return flow south of the filament. This boundary between offshore and onshore flow also corresponds to the temperature front in the SST image of Figure 2C near the southern end of the ship track.

The total geostrophic transport (relative to 480 dbar) through the section is offshore with a magnitude of about 1.7×10^6 m^3/s. This is an underestimate of the total volume transport because the entire velocity field of the filament was not crossed in this survey and the actual depth of the velocity field probably exceeds the reference level of 480 dbar. A deeper penetration of the geostrophic velocity field is indicated in Figure 3C by the slope of the deepest isopycnals: the σ_θ=26.80 surface, for example, has an average slope of about 0.6×10^{-3} across the section. A profile of dynamic height (in dynamic meters) across the section is given at the top of Figure 4B with individual station values indicated by plus (+) signs. The difference in elevation between the sea surface and the 480 dbar surface is about .08 m across this part of the filament and a least square fit, indicated by the solid line, yields a sea surface slope with respect to 480 dbar of 1.5×10^{-6}.

Filaments such as the one observed here are likely to be important in exchanging water masses over the continental shelf along the central California coast. This filament is rooted in a section of the coast between Piedras Blancas to the north (PB in Figure 2C) and Pt. Arguello to the south, a distance of 133 km. The 500 m isobath lies offshore at an average distance of approximately 26 km in this region and the volume shoreward of this line is roughly $9x10^{11}$ m^3. Based on the observed offshore geostrophic transport with respect to 480 dbar, this volume would be exchanged in about 6 days if the filament simply moved the coastal water off shore. This estimate of an exchange time scale is less than the lifetime of the filament derived from the SST imagery of Figure 2. Therefore, the filament persists long enough for such an exchange to occur.

The order of magnitude estimate from the simple exchange model given above indicates that extensive volumes of coastal waters may be affected by the occurrence of these transient filaments. However, the near shore velocity fields of the filaments may be very complex with the exchange being part of a larger scale meandering current system. Such a meandering current system with associated filaments was observed by Ikeda, Mysak and Emery (1984) off Vancouver Island.

4. Instability development and frontal structure

A. SST imagery of instabilities

Following the section of CTD stations across the filament, two high resolution tow-yo surveys were conducted through a pair of instabilities which developed on the southern (cyclonic) front of the filament. During this portion of the experiment, a sequence of four relatively cloud free images was obtained over 19 h which covers the period of development of the instabilities. The times of these images relative to the time intervals of the line of CTD stations (S1) and the tow-yo surveys (S2 and S3) are indicated in Figure 1 by arrows labeled I1 through I4. The first image I1 of the sequence is shown in Figure 5A and was taken on 22 October (JD 295) at 03:57 GMT. The scale of this image is expanded by a factor of four compared with Figures 2A,B,C, and D and the size of individual pixels (1 km) is evident. The instabilities evolve on the frontal feature which stretches from the southeast to the northwest in the image and the positions of the developing instabilities are indicated by arrows numbered 1 and 2.

The second image I2 of the sequence, Figure 5B, shows the same region at 11:37, some 7.5 h after Figure 5A. This image is a subsection of the image of Figure 2C and is indicated in that figure by a rectangle. The initial instability shown by arrow 2 in Figure 5A has evolved into a cusp-like feature in this image. The feature clearly shows two lobes, one warm and one cool, which

appear to wrap around each other in a cyclonic rotation. A second feature which is similar may be seen on this same front farther to the southeast, although this latter feature was not examined in our surveys. Cool surface water may also be seen penetrating northward on the eastern edge of the initial instability indicated by arrow 1; this region of the front is found between the arrows 1 and 2 in Figure 5A. Northwestward propagation of some features of the filament may be seen through careful comparison of Figures 5A and 5B. Two southward extensions of the filament, which are indicated with small arrows along the same front as the instabilities, clearly have a northwestward displacement in Figure 5B compared to Figure 5A. The magnitude of this displacement is about 7 to 9 km over the 7.5 h period. This implies surface velocities between .26 and .34 m/s which are comparable to geostrophic current velocities relative to 480 dbar along the ship track of Figure 2C.

The third image I3 of the sequence is shown in Figure 5C and was taken at 16:19, about 5 h after the image of Figure 5B. At this point, the cool lobe of Instability 2 is more clearly defined while Instability 1 has evolved into a cusp-like feature which is similar to Instability 2. The spacing of these two instabilities along the front is in the range 15 to 20 km and the cross-frontal extent of the warm and cool lobes of Instability 2 is about 8 km. A layer of clouds may be seen intruding into the image from the southwest.

The final image of the sequence I4 taken at 22:58, some 6.5 h after the preceding image, is shown in Figure 5D. Now the warm and cool lobes of Instability 1 have clearly evolved and the entire structure appears to have rotated in a cyclonic sense. An approximate estimate of the cyclonic rotation of Instability 2 is about 14^{o} between images I3 and I4. This implies a rotation rate of about $1x10^{-5}$ s^{-1} or about 0.1f where f is the Coriolis parameter ($f=8.2x10^{-5}$ s^{-1} at this latitude). The cross-frontal extent of Instability 2 has increased somewhat at this point and is now in the range of 9 to 10 km. Clouds obscure much of the sea surface along the western and southern boundaries of the image. Subsequent images over the next several hours are entirely covered with clouds which precludes any further examination of the evolution of the instabilities. The third feature, mentioned above, along this front which resembles Instabilities 1 and 2 and which lies to the southeast appears to be stretching in the along-front direction with very little rotation.

The tracks of the research vessel followed during the two high resolution tow-yo surveys are shown in Figures 6A and 6B. The schematic charts of Figure 6 also show the approximate locations of the 17.6 ^{o}C isotherm at the sea surface obtained from the satellite images of Figures 5C and 5D. This isotherm is chosen because it marks the boundary between the filament and the warmer waters to the south and outlines the instabilities. The latitudes and longitudes which form the rectangles are labeled in

Figure 6A and a scale is included for reference. The boundaries of these diagrams are indicated by rectangles in Figures 5C and 5D. Note that the scale of Figure 5D is slightly larger than the scale of the other images in Figure 5. The first track (S2), indicated with a solid line in Figure 6A, began about two hours after the image I3 was taken at 16:19 as shown in Figure 1. This track is 16.5 km long and took about 3.5 h to complete. A turn to the northeast was executed at the beginning of this track in order to intercept the warm lobe and to position the ship for a southward track through the second instability. The second tow-yo survey (S3), indicated by a solid line in Figure 6B, was underway when the image I4 was taken at 22:58; the ship's position at this time is indicated by an arrow to the right of the ship track. The length of this track is about 28 km and took 5.2 h to complete.

B. Property distributions along ship track S2

A horizontal profile of sea surface temperature along track S2 is shown in Figure 7A and is obtained from the CTD which is "tow-yoed" between about 5 and 110 dbar, typically. The right hand side of the figure is to the northeast. A schematic diagram of a typical section of the "saw tooth" path followed by the CTD through the water column is shown in Figure 8. Points which make up the SST curve (solid line) of Figure 7A are obtained by averaging all temperatures together which lie above

15 dbar for each near surface approach of the CTD; this yields a sea surface temperature about every 500 m along the ship track as indicated in Figure 8. The mixed layer depth is typically 20 to 30 m along these sections so the average temperature above 15 dbar is representative of the mixed layer. Continuous temperature from 2 m depth measured on deck as described in Section 2 is shown with a dashed line in Figure 7A. The agreement between these horizontal temperature profiles indicates that sea surface water properties may be obtained from the CTD used in tow-yo profiling. The difficulties with bubble formation in the continuous 2 m pumped data discussed in Section 2 required this method of extracting sea surface salinity and density. Sea surface salinity along the track is also shown in Figure 7A with a dot-dash line; the salinity scale is given at the right of the figure.

The pattern of warm-cool-warm-cool sea surface temperature in Figure 7A verifies that both lobes of Instability 1 are crossed by the ship track, although just barely. Locating this instability at sea proved difficult because the satellite image used for finding it was a few hours old and the instability itself was moving westward and evolving over the period of these observations. At the beginning of the track in the warm water south of the filament, the sea surface temperature at point (4) is 18.15 $^{\circ}$C. (Only surface temperatures from the 2 m pumping system are available here because the CTD was being raised from the final 500 m cast at Station 10 along S1.) By 3.4 km at point

(3) the surface temperature has dropped to 17.5 °C and is similar to filament temperatures. Farther on at point (2) at 5 km, the surface temperature is back up to 18.19 °C and is close again to temperatures south of the filament. The minimum temperature of 17.35 °C is encountered at about 8 km and may be part of a band of cool water found elsewhere along the front in the satellite images. The temperature and salinity of point (1) which lies at the north end of the track is representative of water properties in the filament. For reference, points (1), (2), (3), and (4) are indicated in the schematic diagram of Figure 6A.

A cross section of isotherms between 10 and 50 dbar along S2 is given in Figure 7B with a contour interval of 0.15 °C. A total of 60 profiles is used in constructing this isotherm map and the spacing between midpoints of adjacent profiles is about 250 m as indicated in Figure 8. The warm waters to the south of the filament are only partially mapped above 30 dbar over the first 3 km, although the 2 m pumped temperature data of Figure 7A indicates that S2 begins in the warm water to the south. The warm lobe of the instability is clearly indicated between 3.7 and 7.3 km by the presence of water above 24 dbar which is warmer than 17.65 °C. To better define the limits of the water to the south of the filament and the position of the warm lobe of the instability, the region between the 17.65 °C and 17.80 °C isotherms is stippled in Figure 7A. Dashed sections of the 17.65, 17.80, and 17.95 °C isotherms are extrapolated to the surface based on the 2 m pumped temperatures. A narrow ribbon of

water cooler than 17.65 °C, which is less than 500 m wide (poorly resolved given the profile spacing) and which extends to the surface, separates the warm southern waters from the warm lobe. This ribbon of cool water is at the edge of the cold lobe of the instability. A distinct doming of isotherms is evident above 30 dbar between 1 and 5 km. The minimum pressure, 21 dbar, of the 17.20 °C isotherm occurs in this region; elsewhere throughout this entire section the 17.20 °C isotherm is found only at greater pressures.

The corresponding map of salinity contoured with an isohaline spacing of 0.01 practical salinity units is shown in Figure 7C. Regions containing salinities between 33.38 and 33.39 have been stippled as before to show where water from south of the filament and from the warm lobe of the instability are found. A much deeper extent of the warm lobe is indicated by the salinity field compared with the temperature field. The stippled region indicating high salinity extends to about 40 dbar between 4 and 6 km while a distict thermal signature of the warm lobe is confined to the upper 24 dbar. The only source of salinities of 33.38 and higher above 40 dbar is the frontal region south of the filament. A region of uplifted isohalines occurs in the same region as the doming of isotherms discussed above. A salinity minimum centered at 45 dbar with minimum salinities of 33.30 is found between 12 and 16 km and may be the signature of intrusive activity occurring in the filament. A broad region of nearly isohaline water is found above 30 dbar north of the high

salinity, warm lobe.

A horizontal profile of σ_θ along track S2 is given in Figure 9A; the dashed section of the profile in the first 3.5 km has been extrapolated based on the 2 m pumped temperature shown in Figure 7A and the surface T-S relation in the warm lobe of the instability. From Figure 9A it is clear that surface temperature gradients also correspond to surface density gradients. The highest surface densities are found in the cool lobe and just northeast of the warm lobe at 8 km. The surface density fronts found here stand in contrast to other observations in which surface thermohaline fronts are encountered on filament boundaries which are nearly compensating in density (cf. Flament et al, 1985). Typically, density compensated fronts are found farther offshore than the frontal regions discussed here.

A map of isopycnals down to 100 dbar is shown in Figure 9B with a contour interval in σ_θ of 0.05 kg/m^3. The similarity of the σ_θ and temperature maps indicates that the water is thermally stratified. The extent of the instability is shown by stippling of regions in the map above 50 dbar for which salinity lies between 33.38 and 33.39. An uplifting of isopycnals which extends down to about 35 dbar is evident under the cool lobe of the instability between 1 and 5 km. A weakening of the seasonal pycnocline is found farther into filament waters beginning at about 13 km. Here the isopycnal spacing increases at around 40 dbar compared to the spacing nearer the beginning of the section.

This high resolution map of the isopycnal field suggests that the slope of the deeper isopycnals increases to the northeast (right-hand side of figure) in the section. Consider the σ_θ = 23.30 surface which has been indicated with a bold line in Figure 9B. While small scale variability in the slope is present, the average slope of this density surface is relatively small over the first 4 to 8 km and then gradually increases over the rest of the section. This change in slope is consistent with lateral shearing of the geostrophic velocity field and in this case the thermal boundary of the filament nearly corresponds to the boundary of the geostrophic flow.

C. Property distributions along ship track S3

Horizontal profiles of surface temperature (solid line) and salinity (dash-dot line) are shown in Figure 10A for segment S3. The ship track is oriented roughly north to south and north is to the left in the figure. Note that the final points at the right or Figures 7 and 9, nearly correspond to the beginning points of track S3. The sea surface temperature pattern of cool-warm-cool-warm indicates that both lobes of the instability are crossed along this ship track. Cooler, low salinity filament water is found at point 1; warmer higher salinity water at point 2 in the warm lobe; cooler, low salinity water at point 3 in the cool lobe; and finally warm, higher salinity water at point 4

which lies to the south of the filament. The four points are labeled 1,2,3, and 4 and correspond to points (1), (2), (3), and (4) in the sea surface temperature and salinity plots of Figure 7A.

A map of isotherms between 10 and 50 dbar along this section is shown in Figure 10B with a contour interval of 0.15 ^{o}C. The map is formed from 114 profiles. The warm lobe of the instability is clearly evident at 18 km in the map where water warmer than 17.50 ^{o}C penetrates down to about 20 dbar. Regions for which the temperature lies between 17.65 and 17.80 ^{o}C are indicated with stippling as before. Waters in the surface layer above 30 dbar are relatively well mixed both in the filament between points 1 and 2 and to the south around point 4. Doming of isothermal surfaces is apparent around 19 km above 30 dbar. The 17.35 ^{o}C isotherm is generally found below 25 dbar throughout the section except for this region of uplifting where it is found at 18 dbar. Water cooler than 17.50 ^{o}C breaks out at the sea surface between about 21 and 22.5 km; these temperatures are encountered elsewhere at the surface only over the first 7 km of the section. Comparison of surface salinities in Figure 10A reveals that, while the temperatures at points 1 and 3 are similar, the salinity at point 3 (33.375) is slightly higher than at point 1 (33.357) which indicates that the water masses are different. While this is not a large salinity difference, it is significant and repeatable (compare the salinities along track S3 between points 1 and 3 with those along track S2 between (1) and

(3)) and is not an artifact of the tow-yo measurement technique.

A deeper penetration of the warm lobe water is again indicated in the contour map of salinity of Figure 10C where salinities exceeding 33.38 are found down to 38 dbar at around 18 km. To better illustrate this, regions of Figure 10C for which salinity lies between 33.38 and 33.39 have again been indicated with stippling. As discussed above, the only source of this relatively saline water is in the frontal region and seasonal thermocline south of the filament. The salinity contour interval in Figure 9C is 0.01. Salinities in the mixed layer and seasonal thermocline within the filament north of the warm lobe are generally less than 33.36. A pool of nearly isohaline water is found above 30 dbar over the first 15 km of the section.

A profile of σ_θ along segment S3 is shown in Figure 11A with a solid line; it is again clear from this profile that surface temperature gradients also correspond to surface density gradients. Points 1,2,3, and 4 are numbered for reference. The isopycnal (σ_θ) field above 100 dbar is given in Figure 11B with an isopycnal contour interval of 0.05 kg/m^3. The extent of the instability is indicated by stippling ($33.38 < S < 33.39$) above 50 dbar. The only points at the surface where σ_θ exceeds 24.15 are in the cold lobe of the instability between 21 and 23.5 km. An uplifting of isopycnals is evident in this same region above 30 dbar. Over the first 23 km the general slope of σ_θ surfaces below 50 dbar is upward to the right in the figure (consistent

with offshore geostrophic flow with respect to 480 dbar). This trend is present for the σ_θ = 25.30 surface, shown with a bold line, which shoals by 20 dbar over the first 23 km of the section. Beyond 23 km, the slope of the 25.30 surface changes sign and produces a slight deepening of this surface in the water south of the filament. A general tendency for isopycnal slopes to become more level below the filament boundary may also be seen for other isopycnal surfaces and again indicates that the water property boundary coincides with the boundary of the geostrophic velocity field of the filament.

D. Near surface stratification

An interesting feature of the near surface layer (pressures less than 15 dbar) along ship track S3 is that water within the warm lobe of this instability is highly stratified compared with surrounding waters in the surface layer. This stratification is found despite 10 m/s winds and 30 m deep mixed layers elsewhere in the section. A plot of the buoyancy frequency N near the surface is shown in Figure 11A with a dash-dot line; the scale for N is on the right-hand side of the figure. Individual values of N are computed from 2 dbar averages of density and sound velocity. Points shown in Figure 11A are averages of all of these individual values above 15 dbar for each near surface approach across the section; this procedure is the same as that used in computing surface water properties discussed

previously. A maximum in N is found at Point 2 in Figure 11A between 17 and 20.5 km with a peak value of 7.3 cycles/hr (cph). Typical maximum values of N in the seasonal thermocline are in the range 15 to 21 cph while mixed layer values are generally less than 1 cph. The secondary peak at 23.3 km is an artifact of the tow-yo sampling scheme and is actually due to a high horizontal gradient of density. A detailed examination of individual profiles throughout both regions of maximum N in Figure 11A reveals that relatively large vertical density gradients are found near the surface at point 2 while at the smaller maximum, water is well mixed to the surface. A somewhat similar near surface increase in N within the cool lobe of Instability 1 may be seen at about 3 km in Figure 9A. Possible mechanisms for producing the observed increases in near surface stratification are given in Section 5.

E. Surface T-S relation

In order to sort out the various surface water mass types, a T-S diagram is constructed along Tracks S2 and S3 and is shown in Figure 12. Points in Figure 12 represent average properties in the upper 15 dbar of the water column. T-S points along Track S2 are shown with a dashed line and points along S3 are shown with a solid line; numbered reference points in this figure are the same as the numbered points in Figures 7A and 10A. Track S2 begins in the cool lobe of Instability 1 (see Figure 6A) at point

(3) and has T-S values that are very similar to those in the cool lobe of Instability 2 along track S3 at the corresponding point 3. Apart from water at point (A), the water at 3 and (3) has the highest density along either track and cannot be formed by simple horizontal mixing of water masses 1 and 4. A straightforward way of accounting for the appearance of "type 3" water at the surface is by local upwelling from a depth of about 30 m. Because temperatures at 1 and 3 are nearly equal, it might be concluded from the SST imagery alone that water at 3 is surface water from the filament which has simply been advected due to the instability. Pure advection, however, would not explain the higher salinity observed at 3. The locus of points on the T-S curve between Points 2 and 3 is almost a straight line and is consistent with strong horizontal mixing across the boundary between the two lobes of Instability 2.

The highest density surface water found is at point (A) which lies north of the warm lobe along track S2. Based solely on the shapes of the T-S curves at points 3, (3), and (A), it might be concluded that similar processes result in the appearance of these water masses at the surface. However, no uplifting of isotherms which might indicate active upwelling is found in association with water mass (A) as may be seen in Figure 7B. Furthermore, the temperature field is more well mixed above 25 dbar at (A) compared with 3 or (3). Water mass (A) is not found along S3.

5. Discussion

Horizontal shear in the near surface velocity field at the cyclonic boundary of the filament is a likely driving mechanism for these instabilities. Although we do not have direct velocity measurements (eg. using an acoustic Doppler velocity profiler), we can estimate the shear in the geostrophic velocity field at the filament boundary from our observations. Below we present horizontal shear estimates based upon the observed velocity difference across the cyclonic front of the filament and upon two length scales: the distance between stations which span the front and an estimate of the width of the shear layer.

The difference in geostrophic velocity averaged between 20 and 40 dbar (within the depth range of the property distributions of the instabilities) relative to 480 dbar computed between Stations 8 and 9 is -0.32 m/s. The distance between these two stations Δy is about 4 km which yields a horizontal shear estimate of $\Delta U/\Delta y \sim -8 \times 10^{-5}\ s^{-1} \sim -f$. This probably represents a lower bound on the actual shear because only the geostrophic component of velocity is used in this estimate and the actual shear scale may be smaller than the station spacing.

An estimate of the shear layer width may be obtained if it is assumed that the along front spacing of the instabilities

equals that of the fastest growing mode of a barotropic distrubance in a uniform shear flow between two regions of constant velocity. The along-front wavenumber k of this mode is specified by $kL \approx 0.4$ where L is half of the shear layer width h (cf. Gill, 1982). From the observed along-front spacing of the instabilities λ of 15 - 20 km (Section 4 and Figure 5), an estimate of the width of the shear layer $h = (0.8/2\pi)\lambda$ is in the range 1.9 to 2.5 km. Therefore, taking h to be of order 2 km along with the velocity difference given above yields a horizontal shear $\Delta U/h \sim -2 \times 10^{-4}\ s^{-1} \sim -2f$. It is interesting that this estimate of h is nearly equal to the width of the surface T-S front on the southern boundary of the filament in Figure 10 A.

It should be pointed out that these order of magnitude shear estimates are subject to error since geostrophic velocities are computed from closely spaced CTD casts (about 8 km). However, as discussed in Section 5, a consistent change in isopycnal slope at the filament boundary is evident over these scales, which indicates strong horizontal shear. Moreover, the order of magnitude estimates given above are comparable to several observations of strong near surface horizontal shear in the range 10^{-4} to 10^{-3} s^{-1} as discussed by Sheres et al (1985). Kosro (1987) reports observations of the velocity field in the upper 200 m of the water column during the Coastal Ocean Dynamics Experiment (CODE) from which horizontal shear may also be estimated. Horizontal shear at the cyclonic boundary of an

upwelling filament off Pt. Arena (see his Figure 4C) and in the along shore current (see his Figure 7B) are both of order 10^{-4} s^{-1}.

The growth rate of these instabilities is consistent with the fastest growing mode of a barotropic disturbance which was assumed above in determining the width of the shear layer. The e-folding time for the growth of a purely barotropic disturbance is about $(0.2\ dU/dy)^{-1}$, cf. Gill (1982), and when evaluated for these observations is about 8 h using the horizontal shear estimate developed above of -2f. While a precise e-folding time is difficult to define from a sequence of satellite images, this is of the same order as the time between images I1 and I3 (12.5 h) in which Instability 1 evolves from a small perturbation on the front into a feature which has two fairly well defined lobes.

The distributions of isopleths of temperature, salinity, and density indicate that the flow field of the instabilities is three-dimensional with local upwelling occuring in the cool lobes of the instabilities. Compensating downwelling presumably occurs on the instability boundaries. Assuming that the σ_θ=24.15 surface which is found at about 30 m (see Figure 11) on either side of the instability migrates to the surface over the time of formation of the instability (1 day), an upwelling rate of about 30 m/day is implied. Following Lee and Atkinson (1983), upwelling within the instabilities can be accounted for based on conservation of potential vorticity,

$$\frac{d}{dt}\left[\frac{\zeta+f}{D}\right] = 0 \qquad (1)$$

where, $$\zeta = \frac{\partial v}{\partial x} - \frac{\partial u}{\partial y}$$

is the relative vorticity, f the planetary vorticity, and D the height of a fluid column. Eastward and northward are the positive x and y directions, respectively.

We hypothesize that as fluid columns move from the narrow region of horizontal shear on the cyclonic boundary of the filament into the frontal instabilities, they undergo a decrease in relative vorticity. To compensate for this decrease in ζ, the height of the fluid columns must also decrease according to (1) so that angular momentum is conserved. The rate at which this decrease in D occurs may be found by differentiating (1) and solving for dD/dt,

$$\frac{dD}{dt} = \left|\frac{D}{\zeta+f}\right| \frac{d\zeta}{dt} \qquad (2)$$

where the change in f with displacement in the y-direction can be neglected.

While insufficient measurements are available to accurately determine the various terms in (2), order of magnitude estimates suggest that changes in ζ might account for the observed upwelling. The initial relative vorticity ζ_1 is taken to be $\zeta_1 \approx -\Delta u/\Delta y \sim -\Delta U/h \sim 2f$ as given above. Idealizing the flow field of the instabilities as irrotational vorticies rotating at angular velocity $\omega_2 \sim 0.1f$ as discussed in Section 4, the relative vorticity within the instabilities is of order

$\varsigma_2 \equiv 2\omega_2 \sim 0.2f$. Further assuming that the time of formation of the instabilities τ is of order one day leads to an estimate of $d\varsigma/dt \sim (\varsigma_2-\varsigma_1)/\tau \sim -2\times10^{-9}\ s^{-2}$. With a mixed layer depth of 30 m, (2) yields an estimate for $dD/dt \sim -18$ m/d which is of the same order as the upwelling rate given above of 30 m/d.

Additional evidence that the velocity fields of the instabilities are three dimensional is the high near surface stratification found within regions of the instabilities, such as in the warm lobe of Instability 2 (see Figure 11A between 17 and 20.5 km). One way an increase in stratification could occur is by near surface vertical shear of the horizontal velocity field across the high gradient frontal region between the instability lobes. This would result in a tilting of isopycnal surfaces from a near vertical orientation initially to an inclined orientation under the influence of the shear; after tilting both vertical and horizontal density gradients would be present. The increase in N to about 8 cph observed in the cool lobe of Instability 1 in Figure 9A at 2.6 km occurs at the edge of a local upwelling region where sloping isopycnals extending to the surface also produce both vertical and horizontal density gradients. Here the upwelling causes isopycnals to rotate from an initial horizontal orientation to one which is more vertical.

Frontal instabilities such as these are probably not important mechanisms for the dissipation of the total kinetic energy of upwelling filaments due to their rather small size and

limited depth. Their overall role in filament dynamics may be as local vertical and horizontal transport mechanisms in horizontal shear layers acting over scales of a few kilometers. They extract kinetic energy from the shear flow at the filament boundary as eddy kinetic energy associated with their rotation and by converting kinetic energy to potential energy through upwelling. They may also be sites of increased dissipation of kinetic energy into heat through the action of small scale turbulent processes. Inasmuch as they are not purely barotropic disturbances, they may also extract available potential energy fron the density field associated with the larger scale geostrophic flow. A crude estimate of the eddy kinetic energy is about 6×10^{8} J (Joules) assuming an eddy to consist of a disc of seawater 4 km in radius rotating at 0.1f and having a vertical extent of about one mixed layer depth (30 m). This is probably an underestimate since the initial rotation rate of the instability may have been larger than 0.1f. An estimate of the potential energy gain through upwelling is larger. Idealizing the cold core of the instabilities as a volume of water 4 km by 4 km by 30 m deep and assuming this volume is raised 30 m into the mixed layer and displaces water which is 0.10 kg/m^3 less dense, the potential energy gain is about 1×10^{10} J. The kinetic energy of the geostrophic flow field of the filament with respect to 480 dbar in Figure 4B is about 3×10^{8} J per m along the axis and for a 100 km long filament yields a total kinetic energy of about 3×10^{13} J. The kinetic energy lost to a single instability, therefore, is less than 0.04 % of the total.

6. Summary and Conclusions

Frontal instabilities were observed on the cyclonic boundary of an upwelling filament which appeared north of Pt. Arguello along the central California coast. The instabilities observed form at an along-frontal wavelength of 15 to 20 km and have a cross-frontal extent of about 8 km. These instabilities are composed of two lobes, one warm and one cool, which rotate about each other in a cyclonic sense. Based on a sequence of satellite SST images, the time scale for instability formation is about 1 day and the relative vorticity within the instabilities is about 0.2 f. The growth rate and along-front wavenumber of these instabilities are consistent with those of the fastest growing mode of a barotropic disturbance in a uniform shear between two regions of constant velocity.

The satellite images were used to direct in situ sampling such that the sub-surface structure of the instabilities could be observed during their evolution. Continuous tow-yo CTD sections through the upper 100 m of the water column were obtained across two instabilites and maps of the temperature, salinity, and density fields are presented. Comparison of the observed in situ SST profiles along the ship tracks with the satellite SST imagery verifies that the instabilities were crossed during shipboard profiling. The depth of penetration of the instabilities appears to be about 40 m based on the salinity field and isopycnal

displacements. Salinity is a better indicator of the vertical extent of the instabilities than either temperature or density. The frontal boundary which separates cool fresher waters of the filament from warmer more saline waters to the south is composed of strong horizontal gradients of temperature, salinity and density. Waters are thermally stratified throughout the regions observed.

The near surface distribution of water properties and finestructure indicates that the velocity field of the instabilities is three dimensional. In particular, a distinct doming of isotherms and isopycnals is found within the cool lobes of the instabilities and is consistent with local upwelling at a rate of about 30 m/day. Surface water masses observed within the cool lobes of the instabilities cannot be formed from advection and simple horizontal mixing of surface waters found inside and outside of the filament. However, a nearly linear T-S relationship is observed for the surface waters between the warm and cool lobes suggesting that strong horizontal mixing processes occur within the instabilities over scales of about 3 km. High stratification ($N > 7$ cph) is observed within the surface layer in the upper 15 m of the water column and may result from vertical shear in the near surface velocity field.

Upwelling within frontal instabilities over horizontal scales of order 5 km may represent an important vertical transport mechanism which acts at filament boundaries. One

effect of this upwelling would be to inject scalars such as nutrients and nearly neutrally buoyant particles, which are initially contained in the seasonal thermocline, into the surface layer in a time period of about 1 day. Due to the sloping isopycnal surfaces within the instabilities, strong isopycnal mixing processes could also transport scalars vertically from the seasonal thermocline into the surface layer. This isopycnal transport could possibly persist even after the larger scale forcing which produced the instabilities has subsided. Clearly, high resolution mapping of the near surface velocity field and mixing processes are needed for a better understanding of the ageostrophic dynamics and transport processes of the instabilities.

In addition to the high resolution tow-yo observations, a section of CTD stations across the filament was obtained and is used to derive a section of the geostrophic velocity field of the filament. The geostrophic velocity field with respect to 480 dbar is that of a baroclinic jet with velocity increasing upwards in the water column. Maximum offshore current velocities are about 0.4 m/s at 60 dbar and the net transport of the filament is at least 1.7 Sv (1 Sv = 10^{-6} m^3/s). This transport is large enough to exchange water masses over large sections of the continental shelf (order 130 km) in a time period which is less than the lifetime of the filament. This indicates that upwelling filaments are important transient circulation mechanisms along the central California coast.

Acknowledgments

We had valuable conversations with Rolf Käse and Pierre Flament during the course of this work. David Siegel, Tom Dickey, and Alan Bratkovich provided helpful comments on a draft of the manuscript. Pierre Flament also developed the software used in processing the satellite images for transmission to the research vessel. Sharon Yamasaki developed much of the software used for CTD data analysis and was responsible for processing and transmitting satellite images during the experiment. Robert Whritner performed the final SST image processing for this manuscript. We thank Walter Richter, Vittorio Barale, Tim Boyd, and Richard Williams for valuable assistance in data collection at sea. We would also like to thank Captain Tom Beattie and the crew of the R/V Ellen B. Scripps for their help in conducting the experiment. All of the satellite images were received and processed at the Scripps Satellite Oceanographic Facility which is partially supported by a block grant from NSF, ONR, and NASA. This work was supported by the Office of Naval Research.

References

Atkinson, L.P., K.H. Brink, R.E. Davis, B.H. Jones, T.

Paluszkiewicz, and D.W. Stuart. Mesoscale hydrographic variability in the vicinity of Points Conception and Arguello during April-May 1983: The OPUS experiment. J. Geophys. Res., 91, C11, 12,899-12918.

Chelton, D.B., R.L. Bernstein, A. Bratkovich, and P.M. Kosro, 1987: The Central California Coastal Circulation Study. EOS, 68 1, i2-13.

Davis, R.E., 1985: Drifter observations of coastal surface currents during CODE: the method and descriptive view. J. Geophys. Res., 90, C3, 4741-4755.

Flament, P.J., L. Armi, and L. Washburn, 1985: The evolving structure of an upwelling filament. J. Geophys. Res., 90, C6, 11765-11778.

Flament, P.J., and L. Armi, 1985: A series of satellite images showing the development of shear instabilities, EOS, 66 (27), cover photo and 523.

Gill, A.E., 1982: Atmosphere-Ocean Dynamics, Academic Press, N.Y., 662 pages.

Huyer A., and P.M. Kosro, 1987: Mesoscale surveys over the shelf and slope in the upwelling region near Pt. Arena. J. Geophys. Res., 92, C2, 1655-1681.

Ikeda, M., L.A. Mysak, and W.J. Emery, 1984: Observation and modeling of Satellite-sensed meanders and eddies off Vancouver Island. J. Phys. Oceanogr., 14, 3-21.

Kosro, P.M., 1987: Structure of the coastal current field off Northern California during the Coastal Ocean Dynamics Experiment. J. Geophys. Res., 92, C2, 1637-1654.

Lee, T.N., 1975: Florida current spin-off eddies. Deep-Sea Res., 22, 753-765.

Lee, T.N., and L.P. Atkinson, 1983: Low-frequency current and temperature variability from Gulf Stream frontal eddies and atmospheric forcing along the Southeast U.S. outer continental shelf. J. Geophys. Res., 88, C8, 4541-4567.

Lee, T.N., L.P. Atkinson, and R. Legeckis, 1981: Observations of a Gulf Steam frontal eddy on the Georgia continental shelf, April 1977. Deep-Sea Res., 28, 4, 347-378.

Lee, T.N., and D. A. Mayer, 1977: Low-frequency current variability and spin-off eddies along the shelf off Southeast Florida. J. Marine Res., 35,1, 193-220.

Narimousa, S., and T. Maxworthy, 1985: Two-layer model of shear-driven coastal upwelling in the presence of bottom topography. J. Fluid Mech., 159, 503-531.

Narimousa, S., and T.Maxworty, 1987: Coastal upwelling on a sloping bottom: the formation of plumes, jets and pinched-off cyclones. J. Fluid Mech., 176, 169-190.

Rienecker, M.M., C.N.K. Mooers, D.E. Hagan, and A.R. Robinson, 1985: A cool anomaly off Northern California: an investigation using IR imagery and in situ data. J. Geophys. Res., 90, C3, 4807-4818.

Sheres, D. and K.E. Kenyon, 1986: Cover photo, EOS, 67, 51.

Sheres, D., K.E. Kenyon, R.L. Bernstein, and R.C. Beardsley, 1985: Large horizontal surface velocity shears in the ocean obtained from images of refracting swell and in situ moored current data, 90, C3, 4943-4950.

Washburn, L. and T.K. Deaton, 1986: A simple system for mapping conductivity microstructure. J. Atmos. and Oceanic Tech., 3, 3, 345-355.

Figure Captions

Figure 1. Upper panel shows time series of wind speed (solid

line) and direction (dased line) from ship's log. Lower panel scale indicates time in Julian days with tic marks every 2 h. Bars above scale show time intervals of CTD survey (S1) and tow-yo surveys (S2 and S3). Arrows above survey bars labeled I1, I2, I3 and I4 give times of SST images shown in Figures 5A,B,C,and D.

Figure 2A. Satellite SST image of area around Pt. Arguello taken at 23:30 GMT on 11 October 1983 (JD 284). Light areas indicate relatively cool water and dark areas indicate warmer water. The point 36 N, 121 W is identified at the top of the image. Spacing between tic marks is 1° in both latitude and longitude.

Figure 2B. As in Figure 2A, but image taken at 22:17 GMT on 17 October 1983 (JD 290).

Figure 2C. As in Figure 2A, but image taken at 11:37 GMT on 22 October 1983 (JD 295). PC is Pt. Conception, PA is Pt. Arguello, PBu is Pt. Buchon, and PB is Piedras Blancas. Ship track across filament for Survey S1 is indicated with a black curve. Area covered by images in Figure 5 is indicated with black rectangle.

Figure 2D. As in Figure 2A, but image taken at 15:14 GMT on 25 October 1983 (JD 298).

Figure 3A. Map of isotherms to 500 dbar for 10 CTD stations of Survey S1. Contour interval is 0.5 $^{\circ}$C. Station locations are shown along top edge of the figure. North is to the left and the x-axis gives relative distance along the ship track.

Figure 3B. As in Figure 3A but, for salinity. Contour interval is 0.05 practical salinity units.

Figure 3C. As in Figure 3A but, for σ_θ. Contour interval is 0.10 kg/m^3.

Figure 4A. Profiles of geostrophic velocity computed with respect to 480 dbar between various stations of Survey S1. Labels identify stations used in computing profiles. Positive velocities indicate onshore flow.

Figure 4B. Upper panel gives dynamic height in m for 0 dbar with respect to 480 dbar for the 10 stations of Survey S1. Individual values are indicated with plus (+) signs and the solid line is a least squares fit. Lower panel is a map of isotachs of geostrophic velocity for Survey S1 in m/s computed with respect to 480 dbar. Stippled areas indicate onshore flow.

Figure 5A. SST Image I1 of area enclosed by rectangle in Figure 2C taken at 03:57 on 22 October 1983 (JD 295). Shading as in Figure 2A. Arrows 1 and 2 indicate developing frontal

instabilities.

Figure 5B. As in Figure 5A, but for Image I2 taken at 11:37.

Figure 5C. As in Figure 5B, but for Image I3 taken at 16:19. Black rectangle encloses area shown in schematic of Figure 6A.

Figure 5D. As in Figure 5A, but for Image I4 taken at 22:58. Black rectangle encloses area shown in schematic of Figure 6B. Scale of this image is slightly larger than that of Figures 5A, 5B, and 5C.

Figure 6A. Schematic diagram showing ship tracks S2 (solid line) and S3 (dashed line) in relation to instabilities at 16:19 GMT on 22 October 1983. Instabilities are outlined by the 17.6 ^{o}C isotherm which is shown with a solid line. Points (1) through (4) are also indicated in the T,S, and σ_θ profiles of Figures 7A and 9A. Position of area shown here is indicated by rectangle in satellite SST image of Figure 5C.

Figure 6B. As in 6A, but at 22:58 GMT on 22 October 1983. Points 1 through 4 are also indicated in the T,S, σ_θ profiles of Figures 10A and 11A. Position of area shown here is indicated by rectangle in SST image of Figure 5D. Arrow to right of ship track S3 indicates postion of research vessel when image shown in Figure 5D was taken.

Figure 7A. Horizontal profiles of temperature (solid line) and salinity (dash-dot line) averaged over upper 15 dbar obtained from profiling CTD along ship track S2. Continuous sea surface temperature (dashed line) at 2m depth is labeled as T_{2m}. Points (1) through (4) are indicated in relation to instabilities in Figure 6A. Direction of Section S2 indicated by SW (southwest) and NE (northeast) at top of figure.

Figure 7B. Map of isotherms between 10 and 50 dbar along ship track S2. Contour interval is 0.15 $^{\circ}$C. Temperatures between 17.65 and 17.80 $^{\circ}$C are stippled.

Figure 7C. As in 7B, but for salinity. Contour interval is 0.01. Salinities between 33.38 and 33.39 are stippled.

Figure 8. Diagram of "saw tooth" tow-yo path followed by profiling CTD.

Figure 9A. As in Figure 7A, but for σ_θ (solid line) and bouyancy frequency N (dash-dot line).

Figure 9B. As in Figure 7B, but for σ_θ between 10 and 100 dbar. Contour interval is 0.05 kg/m^3. Stippling as in Figure 7C. Bold line indicates σ_θ = 25.30 surface.

Figure 10A. As in Figure 7A, but for ship track S3. Points 1 through 4 are indicated in relation to instabilities in Figure 6B. Direction of Section S3 indicated by N (north) and S (south) at top of figure.

Figure 10B. As in Figure 7B, but for ship track S3.

Figure 10C. As in Figure 7C, but for ship track S3.

Figure 11A. As in Figure 9A, but for ship track S3.

Figure 11B. As in Figure 9B, but for ship track S3.

Figure 12. Surface T-S diagram for points in Figures 7A (dashed line) and 10A (solid line). Points (1) through (4) and 1 through 4 are shown in relation to instabilities in Figures 6A and 6B..

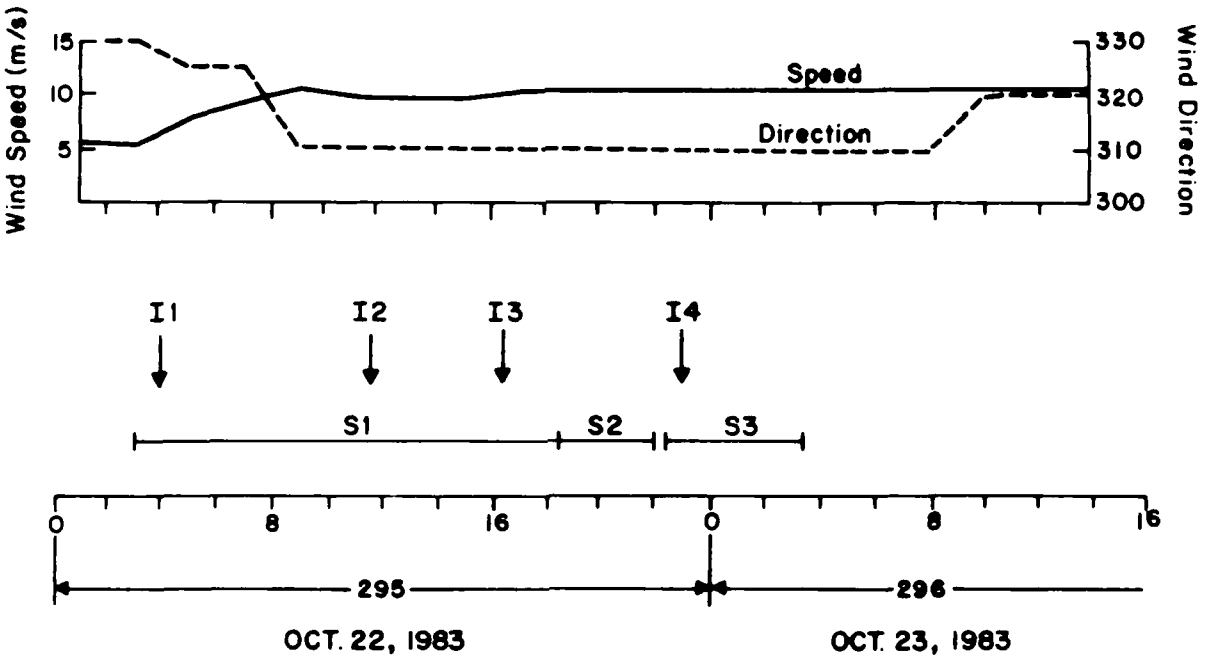
Wind Speed (m/s)
15
10
5
Speed
Direction
330
320
310
300
Wind Direction
I1
I2
I3
I4
S1
S2
S3
0
8
16
0
8
16
295
296
OCT. 22, 1983
OCT. 23, 1983

Figure 1

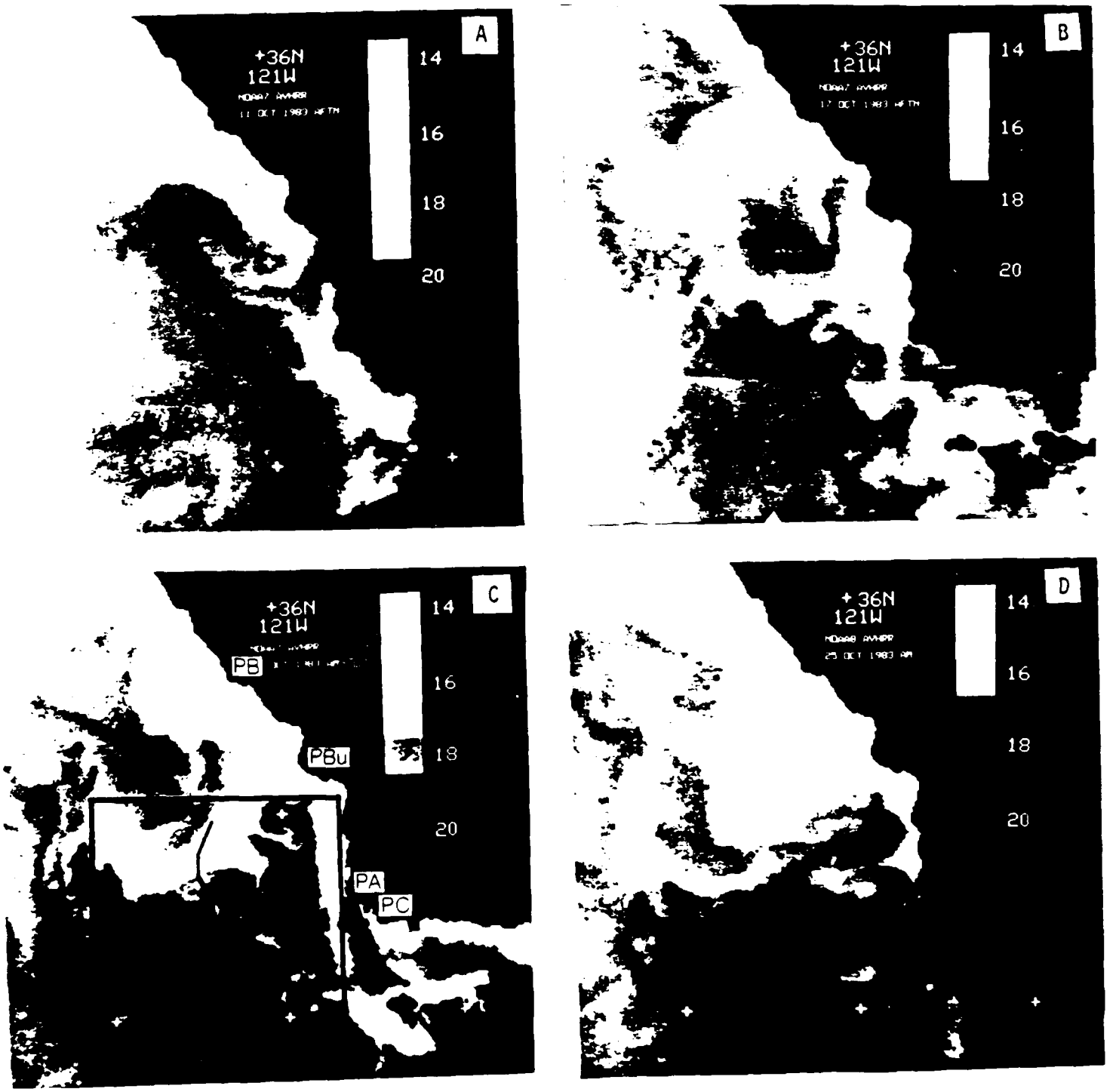
A
+36N
121W
14
16
18
20
B
+36N
121W
14
16
18
20
C
+36N
121W
PB
PBu
PA
PC
14
16
18
20
D
+36N
121W
14
16
18
20

Figure 2

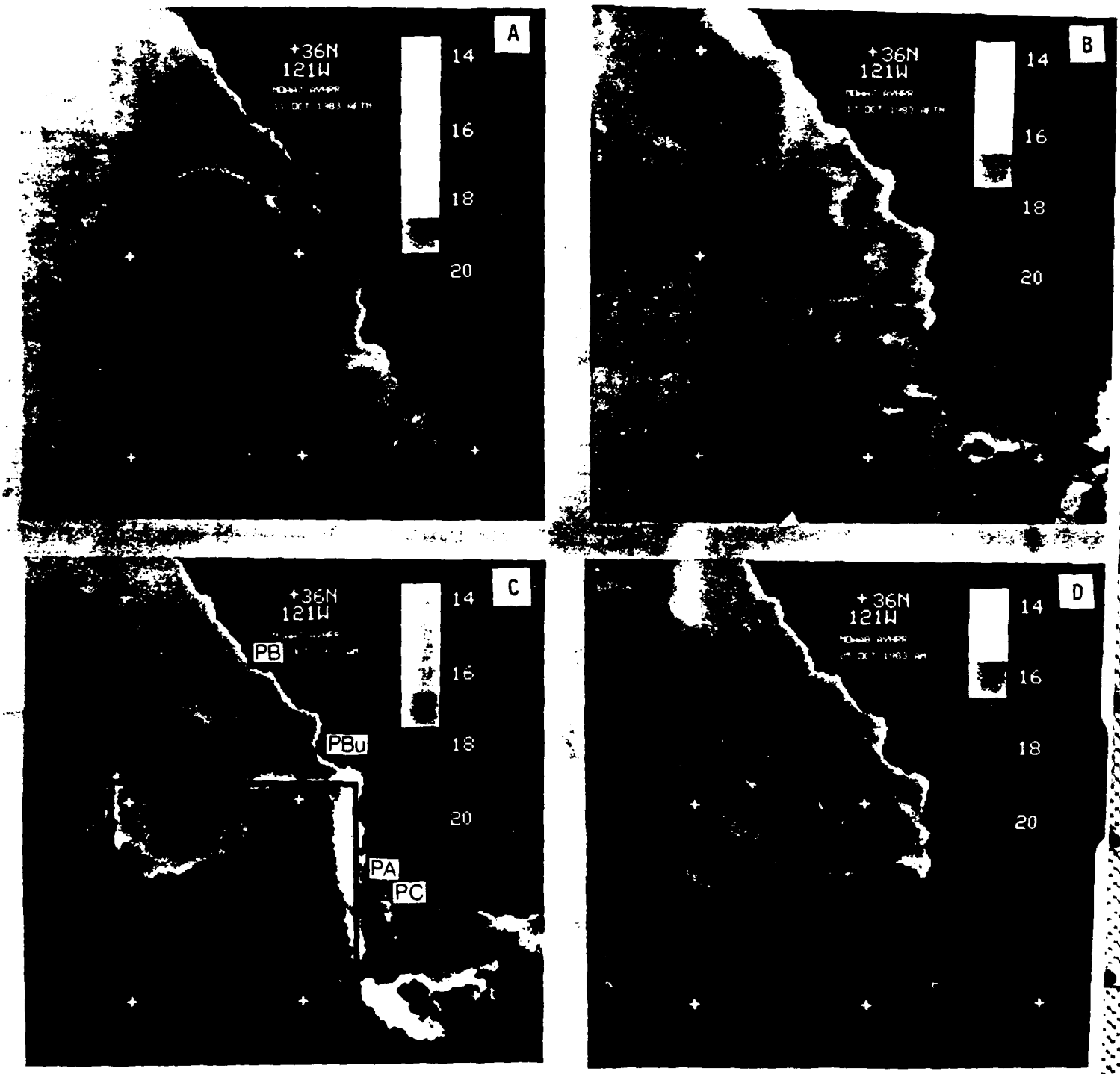
A
+36N
121W
14
16
18
20
B
+36N
121W
14
16
18
20
C
+36N
121W
14
16
18
20
PB
PBu
PA
PC
D
+36N
121W
14
16
18
20

Figure 2

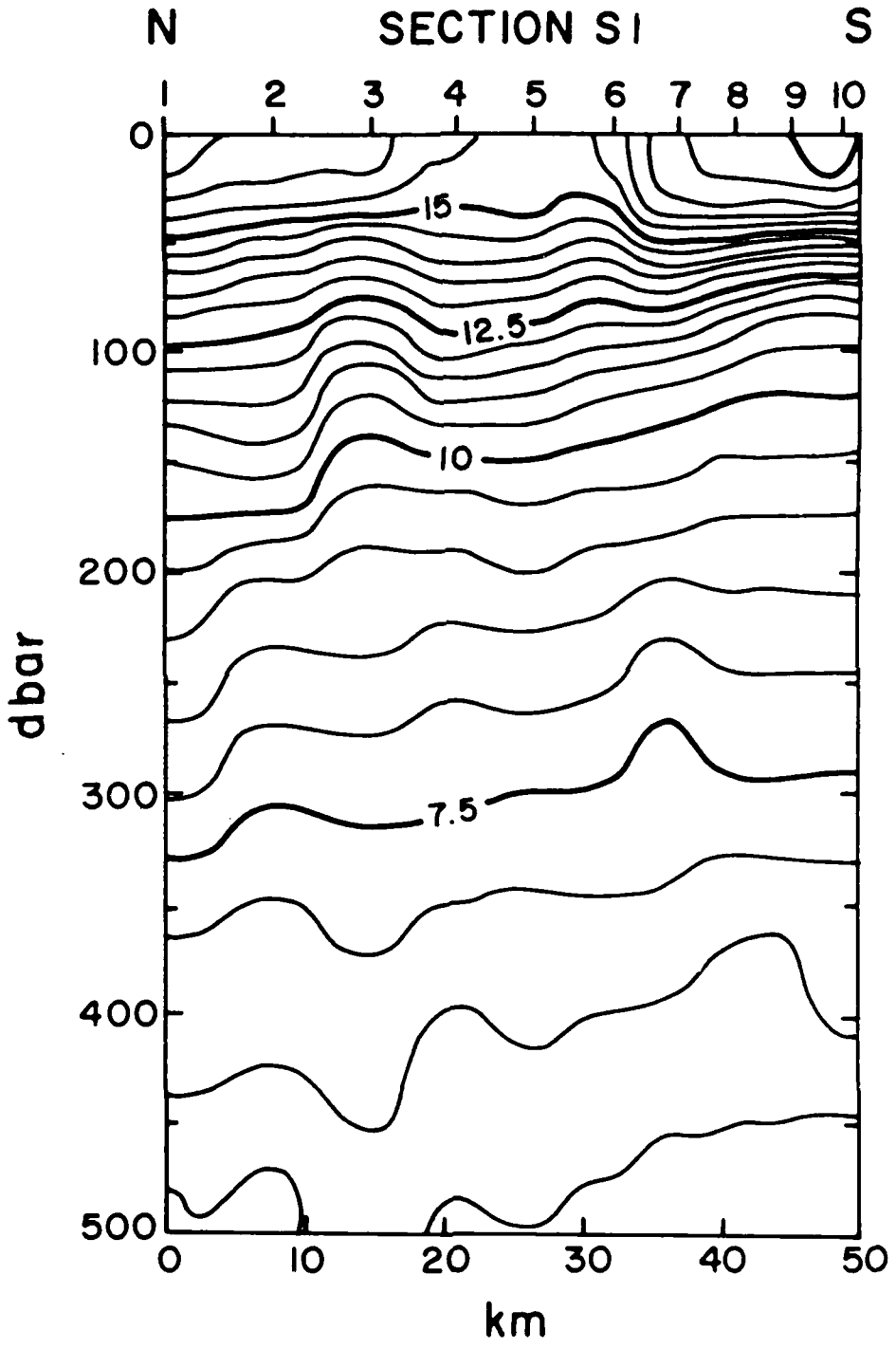
N
SECTION S1
S
1
2
3
4
5
6
7
8
9
10
0
100
200
300
400
500
dbar
15
12.5
10
7.5
0
10
20
30
40
50
km

Figure 3A

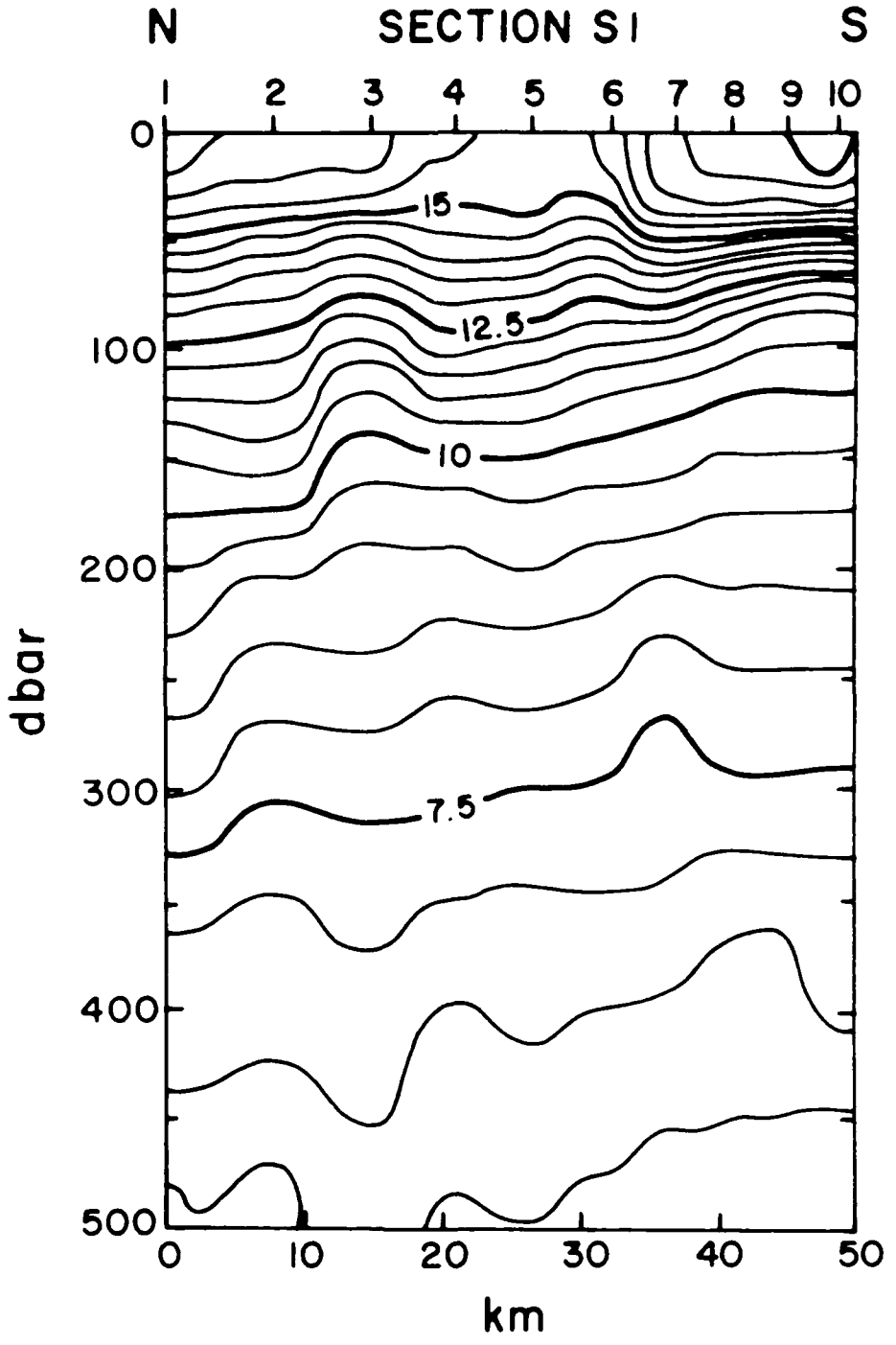
N
SECTION S1
S
1
2
3
4
5
6
7
8
9
10
0
100
200
300
400
500
dbar
15
12.5
10
7.5
0
10
20
30
40
50
km

Figure 3A

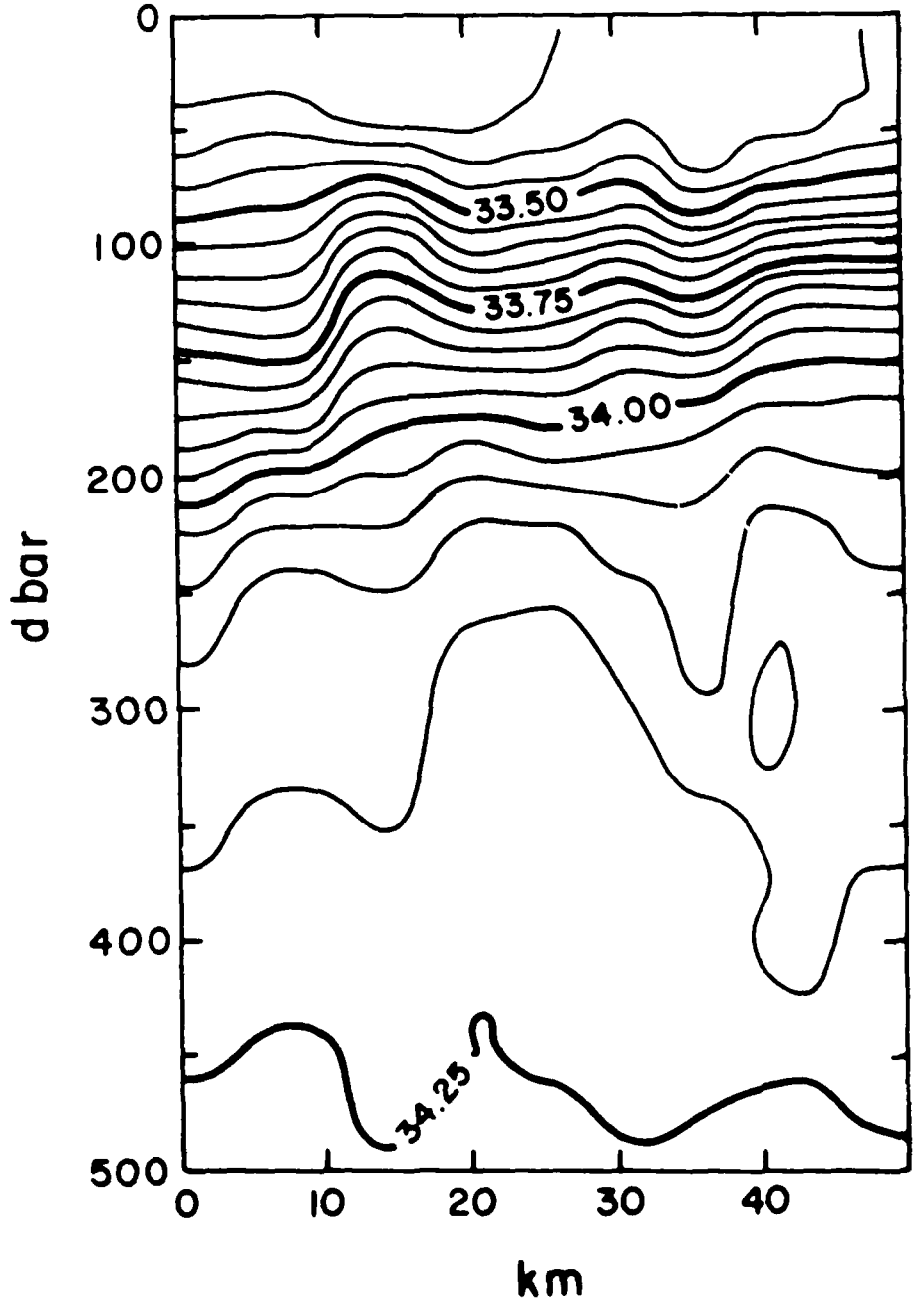

Figure 3B

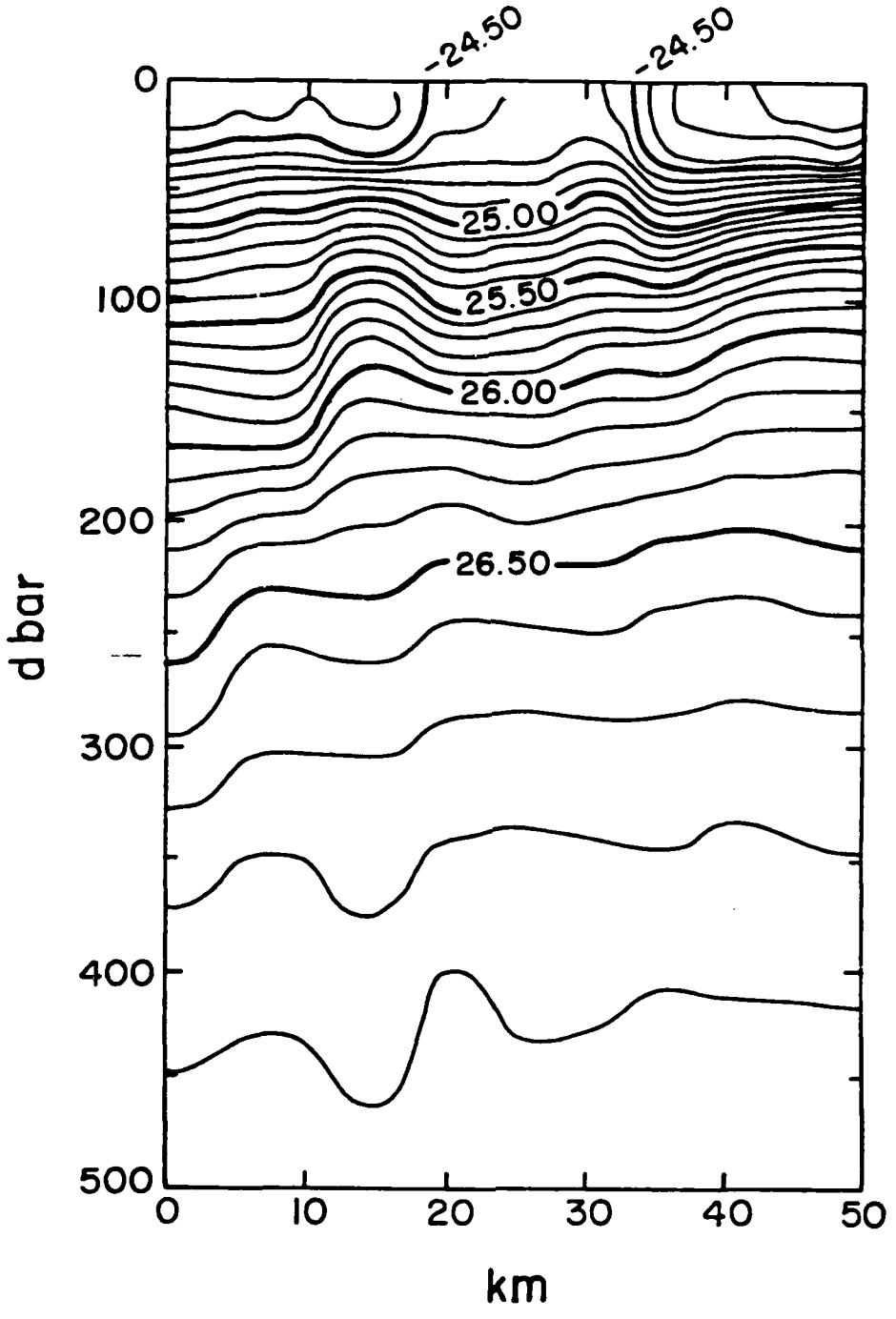
-24.50
-24.50
0
25.00
100
25.50
26.00
200
26.50
d bar
300
400
500
0
10
20
30
40
50
km

Figure 3C

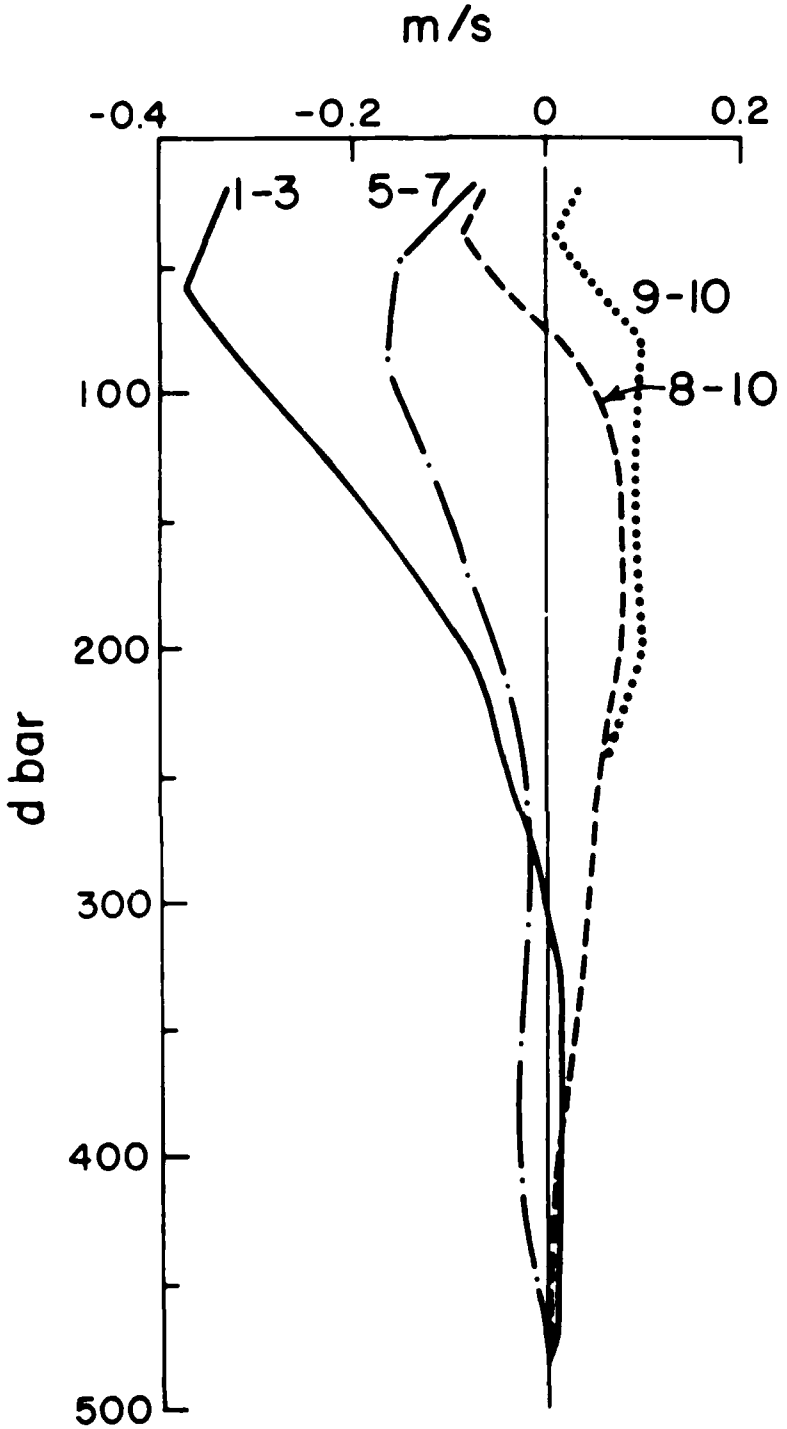

Figure 4A

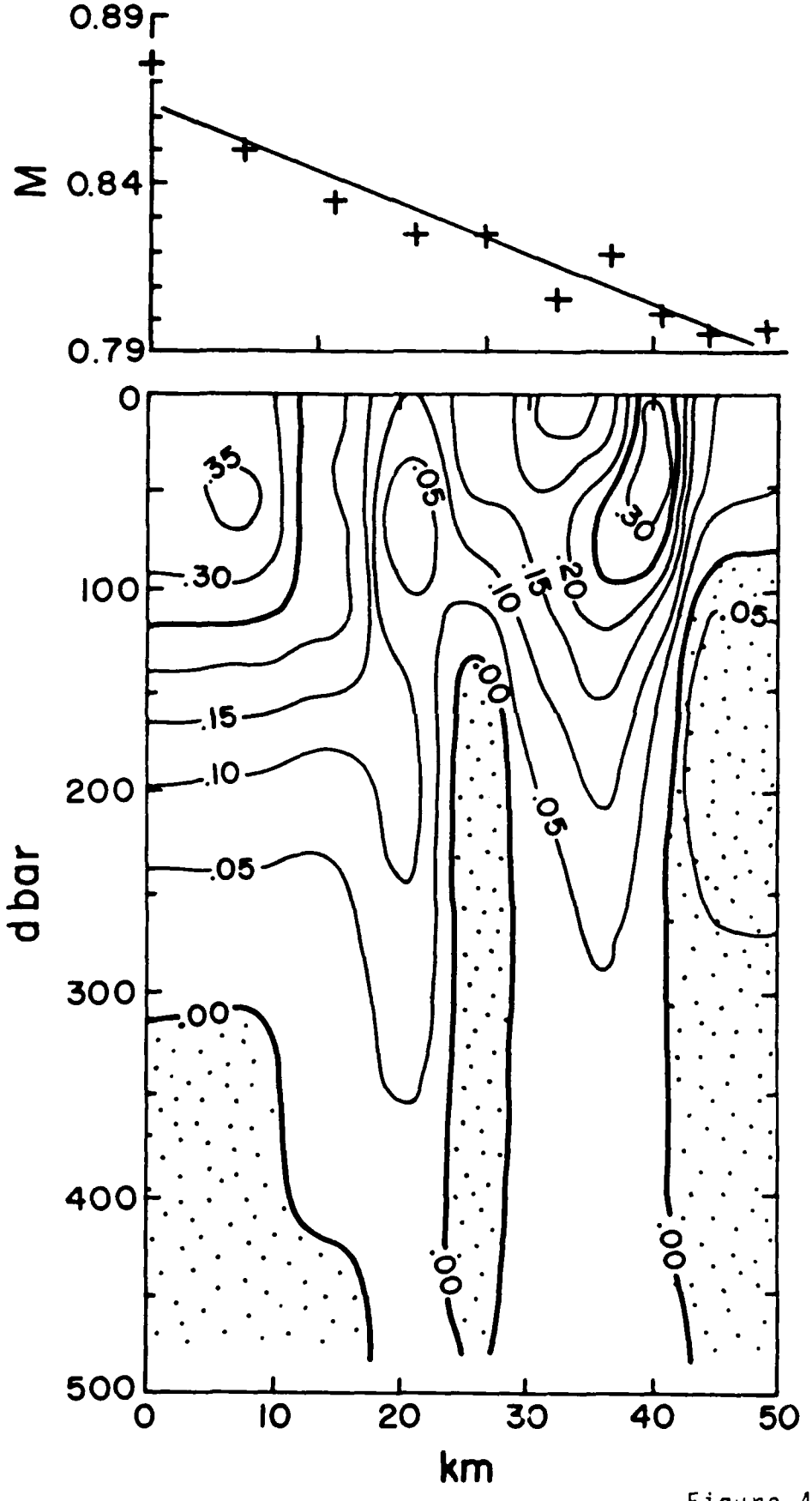
0.89
M
0.84
0.79
0
100
200
300
400
500
dbar
35
30
25
20
15
10
05
00
0
10
20
30
40
50
km

Figure 48

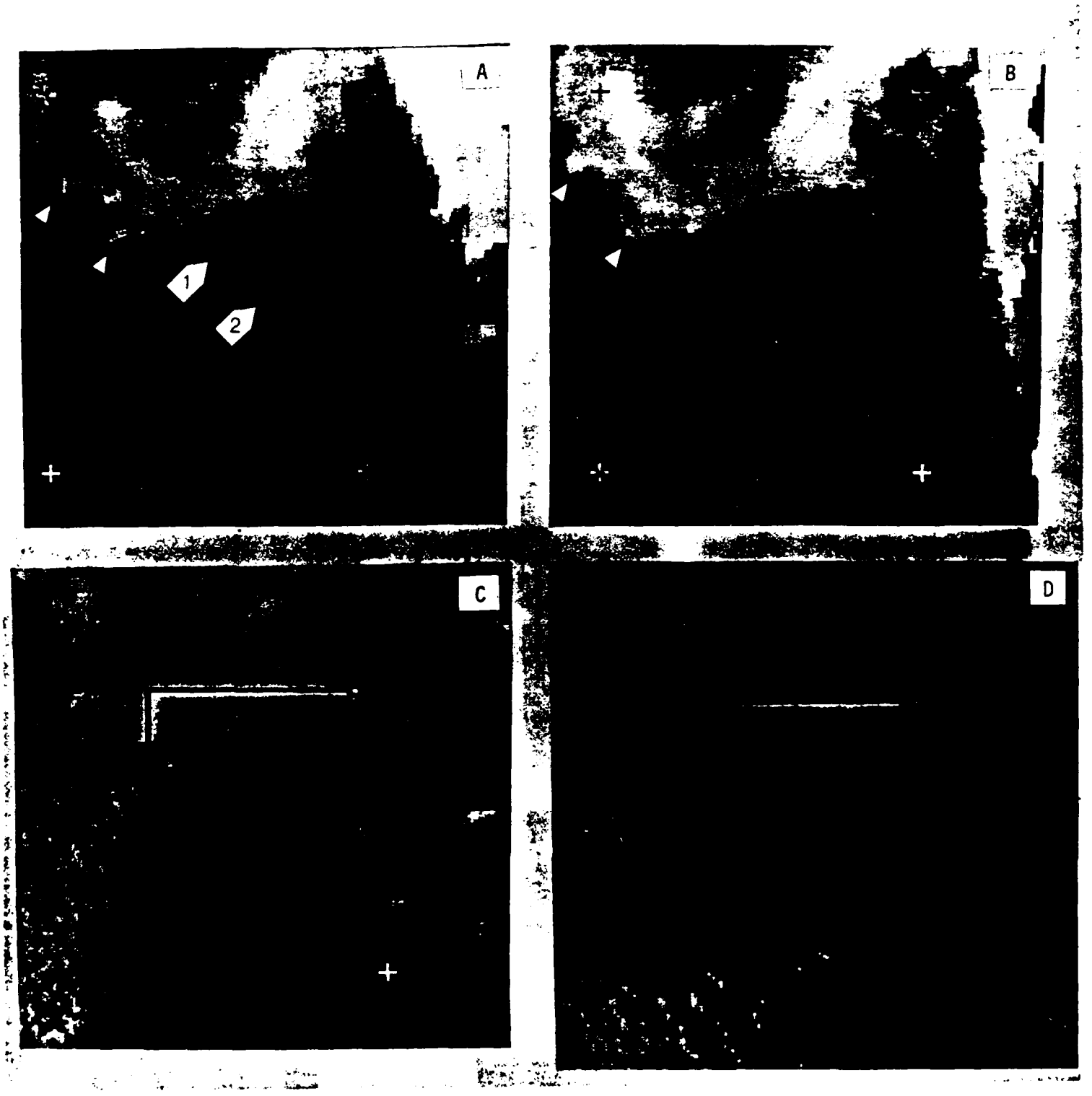

Figure 5

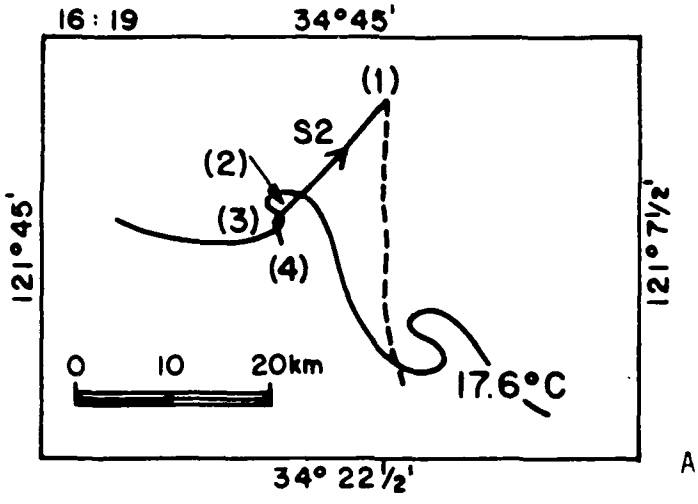
16:19
34°45'
(1)
S2
(2)
(3)
(4)
121°45'
121°7½'
0
10
20km
17.6°C
34° 22½'

A

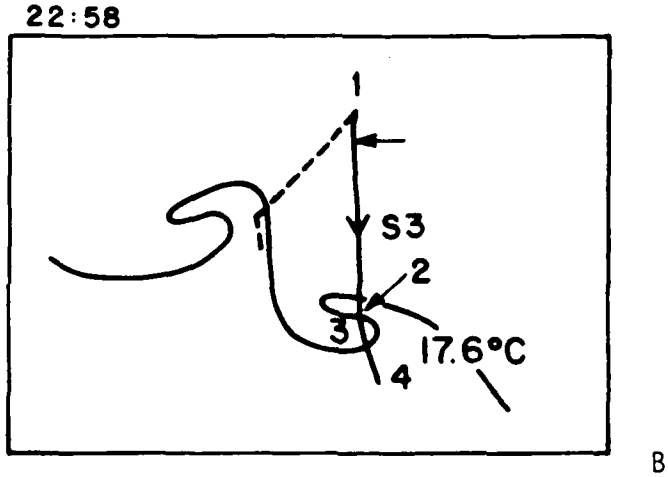
22:58
1
S3
2
3
4
17.6°C

B

Figure 6

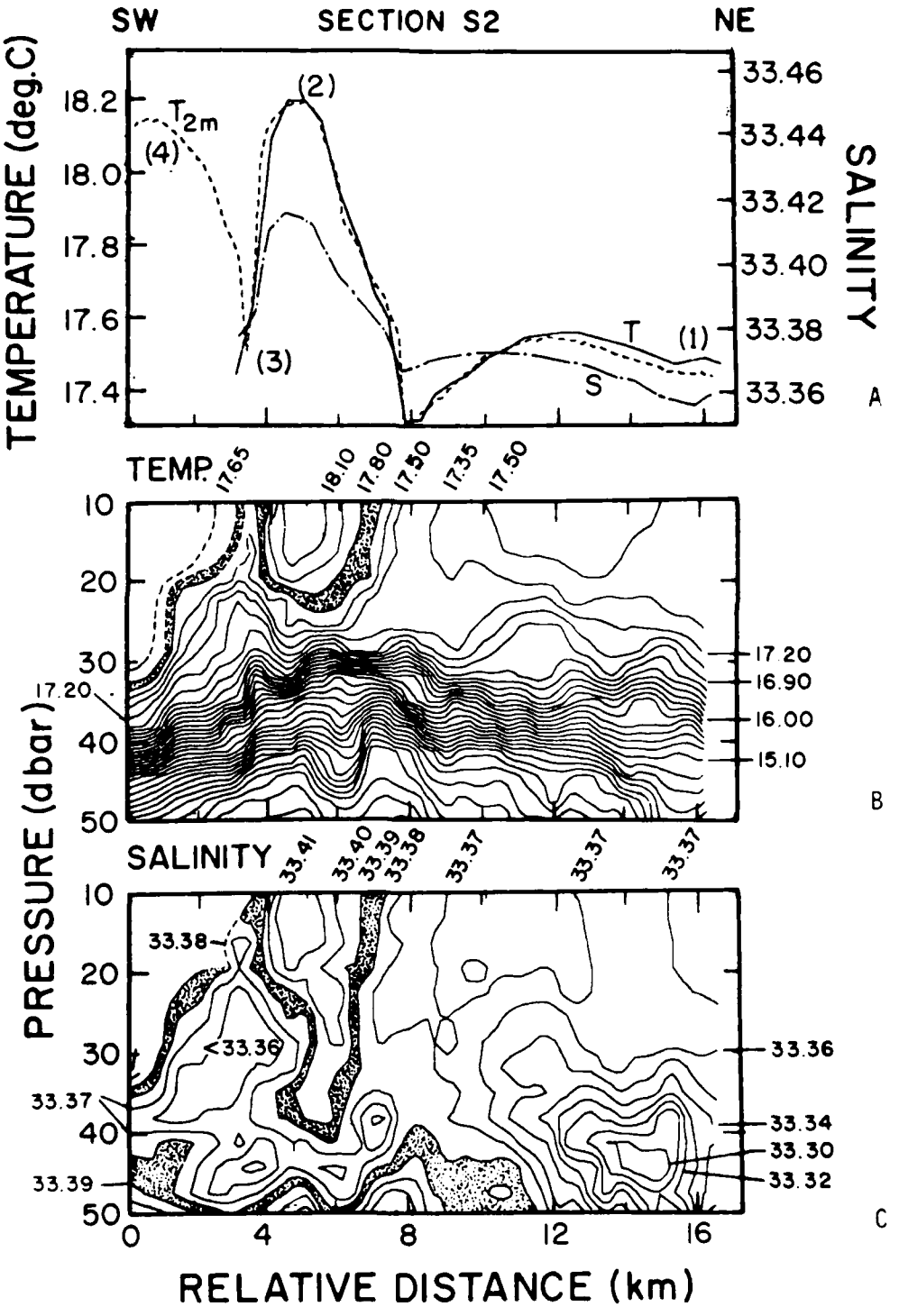
SW
SECTION S2
NE
TEMPERATURE (deg.C)
SALINITY
18.2
18.0
17.8
17.6
17.4
33.46
33.44
33.42
33.40
33.38
33.36
T_{2m}
(1)
(2)
(3)
(4)
T
S
A
TEMP.
17.65
18.10
17.80
17.50
17.35
17.50
10
20
30
40
50
17.20
16.90
16.00
15.10
PRESSURE (dbar)
B
SALINITY
33.41
33.40
33.39
33.38
33.37
33.37
33.37
33.38
33.36
33.37
33.39
33.36
33.34
33.30
33.32
C
0
4
8
12
16
RELATIVE DISTANCE (km)

Figure 7

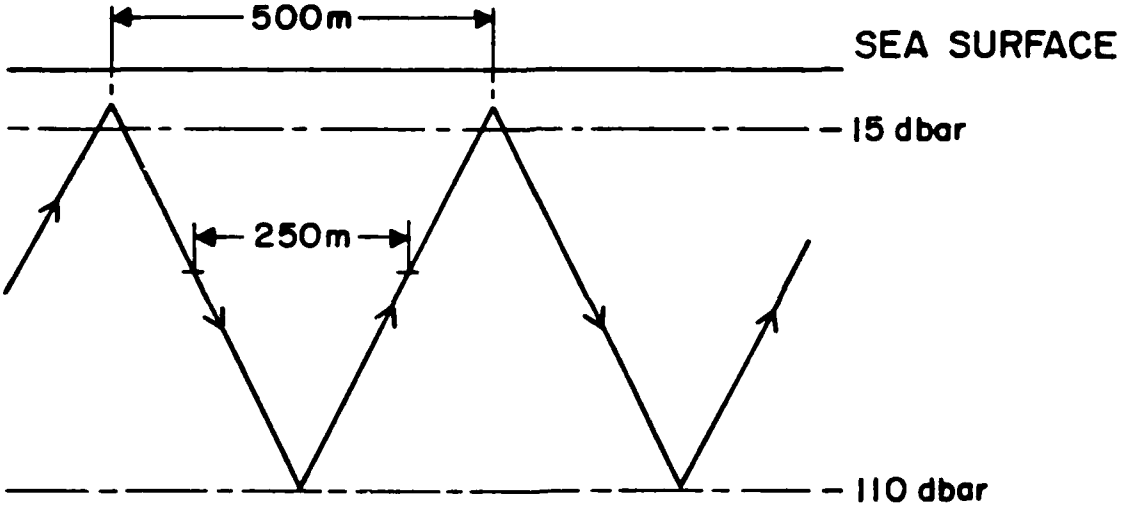

Figure 8

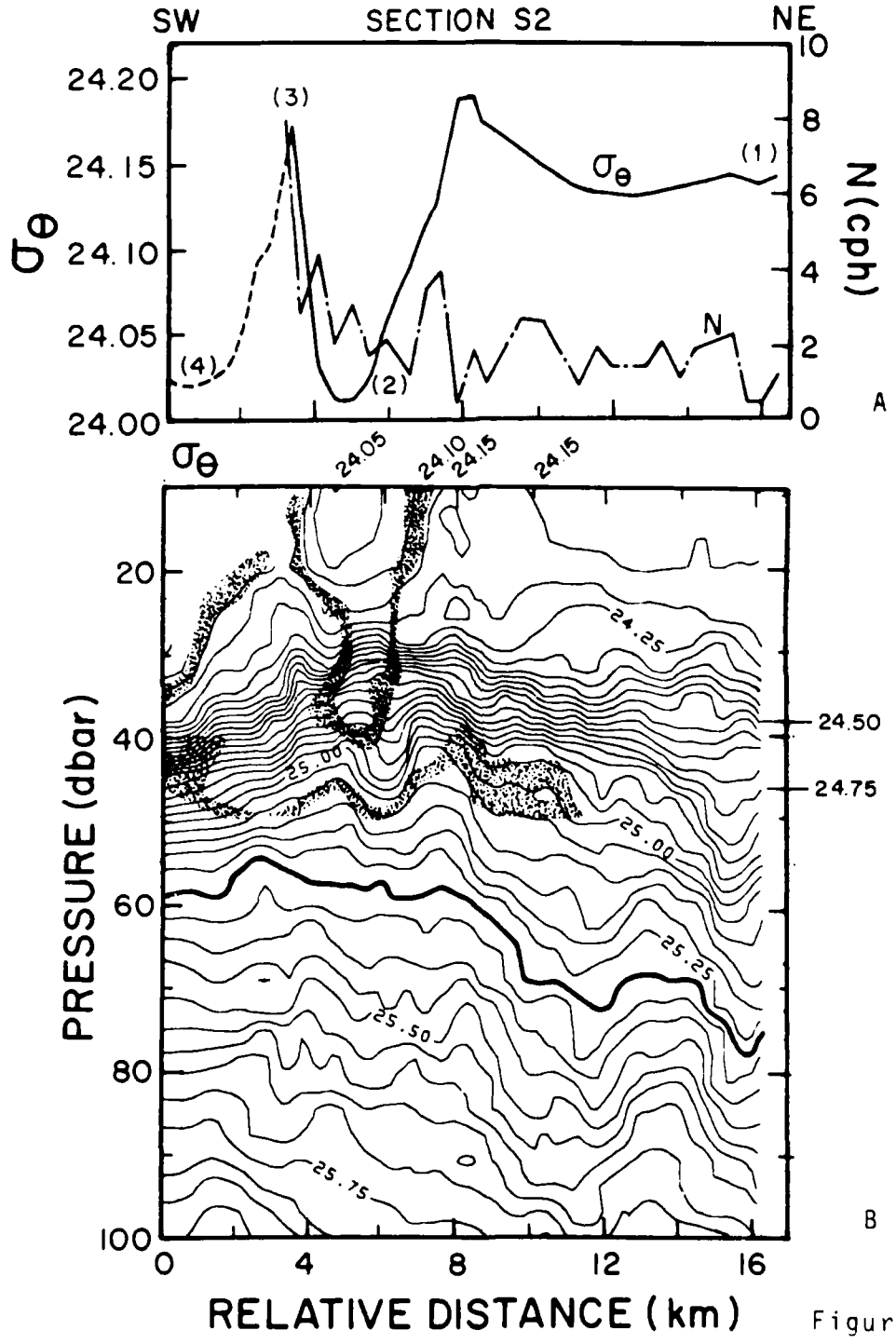
SW
SECTION S2
NE
24.20
24.15
24.10
24.05
24.00
σθ
(3)
(4)
(2)
(1)
σθ
N
10
8
6
4
2
0
N (cph)
A
σθ
24.05
24.10
24.15
24.15
20
40
60
80
100
PRESSURE (dbar)
24.25
25.00
25.00
25.25
25.50
25.75
24.50
24.75
B
0
4
8
12
16
RELATIVE DISTANCE (km)

Figure 9

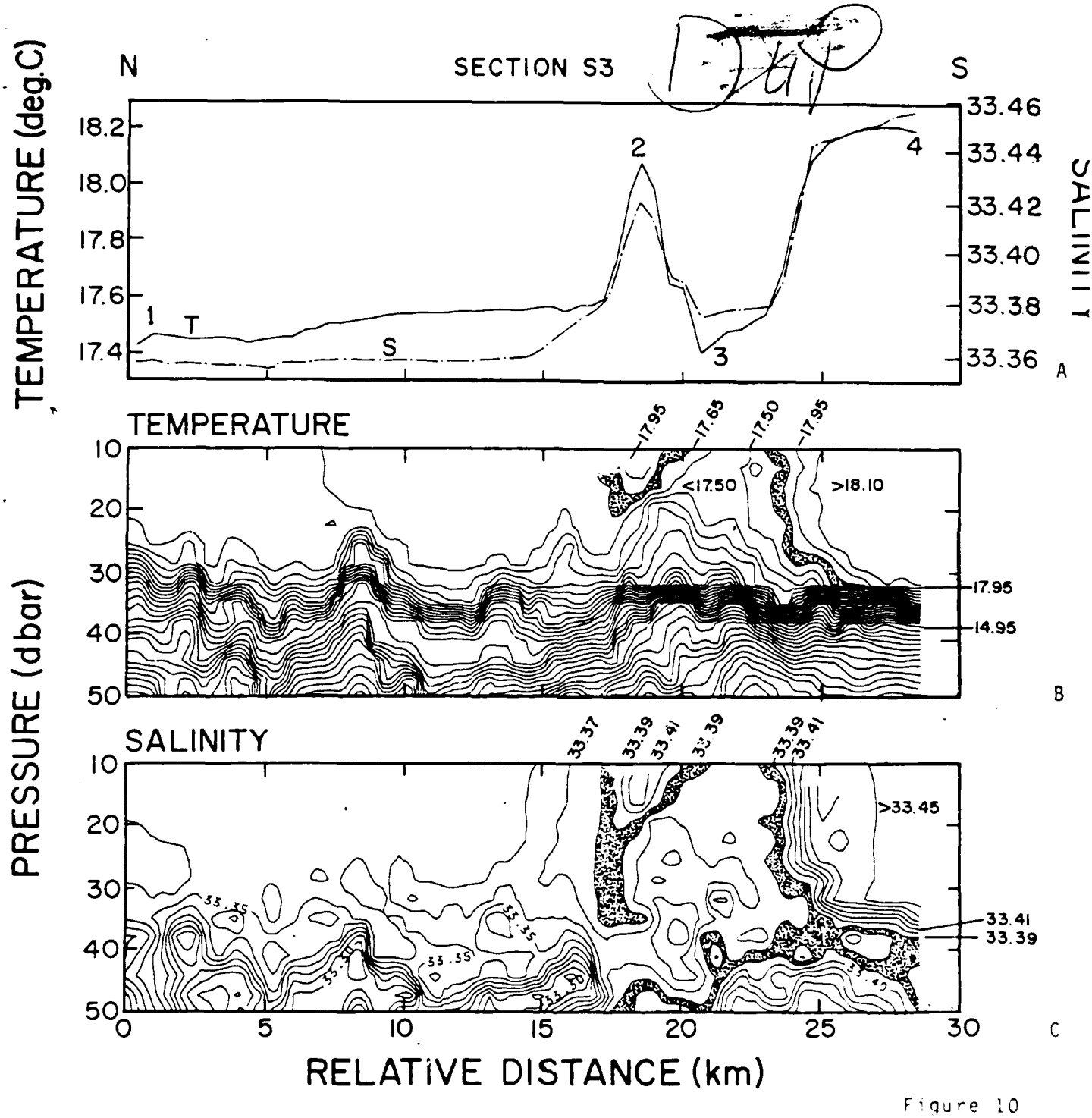
N
SECTION S3
S
TEMPERATURE (deg.C)
SALINITY
18.2
18.0
17.8
17.6
17.4
33.46
33.44
33.42
33.40
33.38
33.36
1
T
S
2
3
4
A
TEMPERATURE
17.95
17.65
17.50
17.95
<17.50
>18.10
17.95
14.95
B
SALINITY
33.37
33.39
33.41
33.39
33.39
33.41
>33.45
33.41
33.39
C
PRESSURE (dbar)
10
20
30
40
50
0
5
10
15
20
25
30
RELATIVE DISTANCE (km)

Figure 10

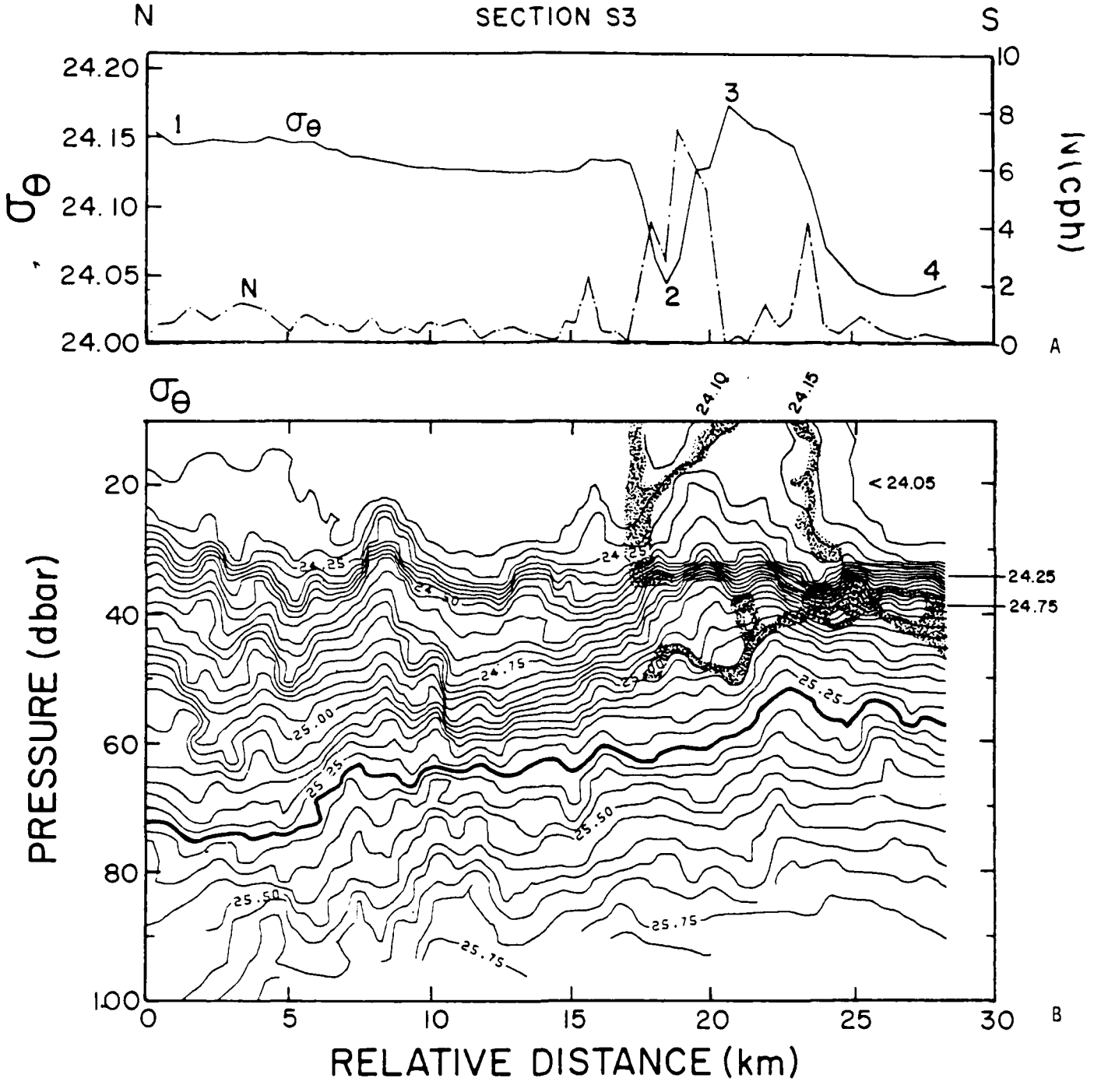
N
SECTION S3
S
24.20
24.15
24.10
24.05
24.00
σθ
1
σθ
2
3
4
N
10
8
6
4
2
0
N(cph)
A
σθ
24.10
24.15
< 24.05
24.25
24.75
PRESSURE (dbar)
20
40
60
80
100
0
5
10
15
20
25
30
B
RELATIVE DISTANCE (km)

Figure 11

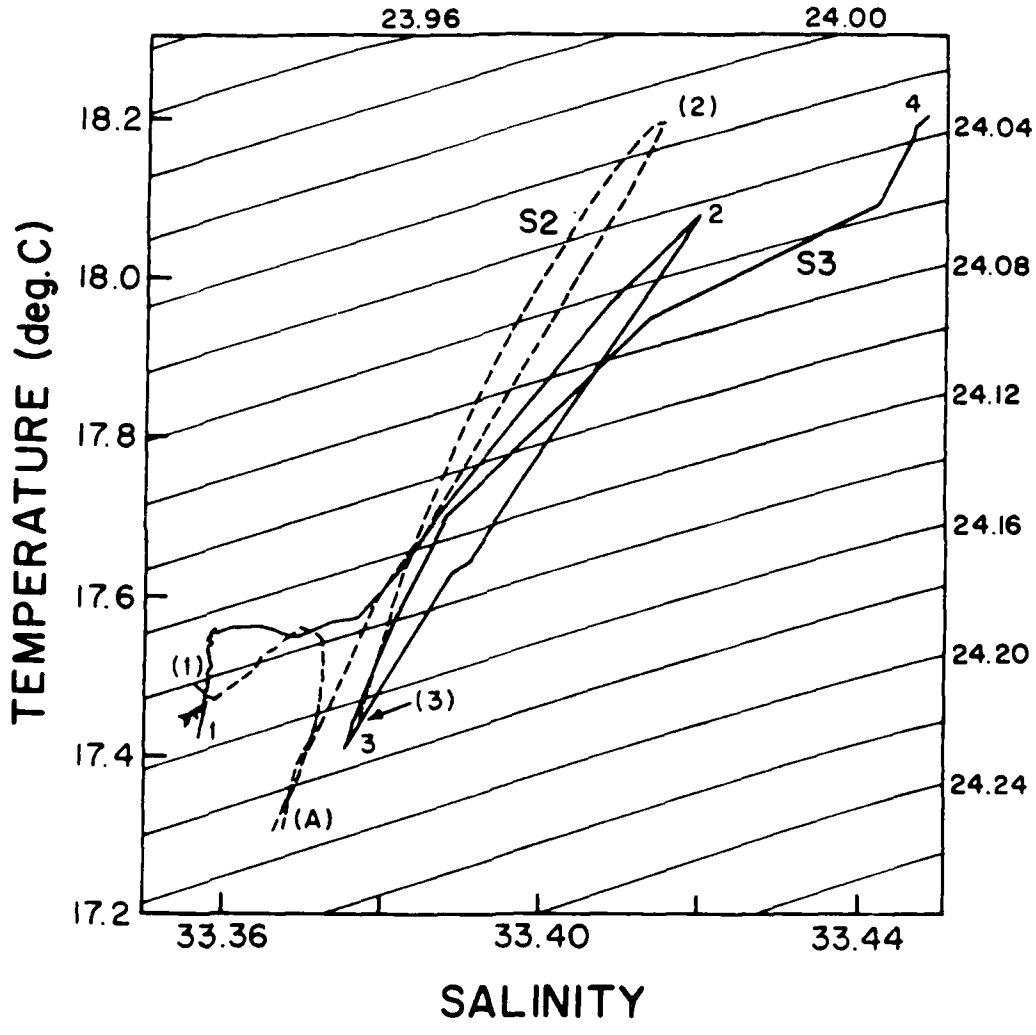
23.96
24.00
18.2
18.0
17.8
17.6
17.4
17.2
TEMPERATURE (deg.C)
24.04
24.08
24.12
24.16
24.20
24.24
33.36
33.40
33.44
SALINITY
(1)
(2)
(3)
(A)
1
2
3
4
S2
S3

Figure 12

END

DATE

FILMED

5-88

DTIC